

# *Increasingly seasonal jet stream raises risk of co-occurring flooding and extreme wind in Great Britain*

Article

Published Version

Creative Commons: Attribution 4.0 (CC-BY)

Open Access

Hillier, J. K. ORCID: <https://orcid.org/0000-0002-0221-8383>,  
Bloomfield, H. C., Manning, C., Garry, F. ORCID:  
<https://orcid.org/0000-0002-9640-6675>, Shaffrey, L. ORCID:  
<https://orcid.org/0000-0003-2696-752X>, Bates, P. and Kumar, D. ORCID: <https://orcid.org/0000-0003-2253-4129> (2025)  
Increasingly seasonal jet stream raises risk of co-occurring  
flooding and extreme wind in Great Britain. International  
Journal of Climatology, 45 (5). e8763. ISSN 1097-0088 doi:  
10.1002/joc.8763 Available at  
<https://centaur.reading.ac.uk/121788/>

It is advisable to refer to the publisher's version if you intend to cite from the work. See [Guidance on citing](#).

To link to this article DOI: <http://dx.doi.org/10.1002/joc.8763>

Publisher: Wiley

the [End User Agreement](#).

[www.reading.ac.uk/centaur](http://www.reading.ac.uk/centaur)

**CentAUR**

Central Archive at the University of Reading

Reading's research outputs online

RESEARCH ARTICLE OPEN ACCESS

# Increasingly Seasonal Jet Stream Raises Risk of Co-Occurring Flooding and Extreme Wind in Great Britain

John K. Hillier<sup>1</sup>  | Hannah C. Bloomfield<sup>2</sup> | Colin Manning<sup>2</sup> | Freya Garry<sup>3</sup>  | Len Shaffrey<sup>4,5</sup> | Paul Bates<sup>6,7</sup> | Dhirendra Kumar<sup>4</sup>

<sup>1</sup>Department of Geography and Environment, Loughborough University, Loughborough, UK | <sup>2</sup>School of Engineering, Newcastle University, Newcastle, UK | <sup>3</sup>Met Office, Exeter, UK | <sup>4</sup>Department of Meteorology, University of Reading, Reading, UK | <sup>5</sup>National Centre for Atmospheric Science, University of Reading, Reading, UK | <sup>6</sup>School of Geographical Sciences, University of Bristol, Bristol, UK | <sup>7</sup>Cabot Institute, University of Bristol, Bristol, UK

**Correspondence:** John K. Hillier ([j.hillier@lboro.ac.uk](mailto:j.hillier@lboro.ac.uk))

**Received:** 2 July 2024 | **Revised:** 5 December 2024 | **Accepted:** 13 January 2025

**Funding:** This work was supported by UK Research and Innovation.

**Keywords:** episodes | extreme wind | flooding | insurance risk | jet stream | multi-hazard | seasonality | storms

## ABSTRACT

Insurers and risk managers for critical infrastructure such as transport or power networks typically do not account for flooding and extreme winds happening at the same time in their quantitative risk assessments. We explore this potentially critical underestimation of risk from these co-occurring hazards through studying events using the regional 12 km resolution UK Climate Projections for a 1981–1999 baseline and projections of 2061–2079 (RCP8.5). We create a new wintertime (October–March) set of 3427 wind events to match an existing set of fluvial flow extremes and design innovative multi-event episodes ( $\Delta t$  of 1–180 days long) that reflect how periods of adverse weather affect society (e.g., through damage). We show that the probability of co-occurring wind-flow episodes in Great Britain (GB) is underestimated 2–4 times if events are assumed independent. Significantly, this underestimation is greater both as severity increases and episode length reduces, highlighting the importance of considering risk from closely consecutive storms ( $\Delta t \sim 3$  days) and the most severe storms. In the future (2061–2079), joint wind-flow extremes are twice as likely as during 1981–1999. Statistical modelling demonstrates that changes may significantly exceed thermodynamic expectations of higher river flows in a wetter future climate. The largest co-occurrence increases happen in mid-winter (DJF) with changes in the North Atlantic jet stream an important driver; we find the jet is strengthened and squeezed into a southward-shifted latitude window ( $45^\circ$ – $50^\circ$  N) giving typical future conditions that match instances of high flows and joint extremes impacting GB today. This strongly implies that the large-scale driving conditions (e.g., jet stream state) for a multi-impact ‘perfect storm’ will vary by country; understanding regional drivers of weather hazards over climate timescales is vital to inform risk mitigation and planning (e.g., diversification and mutual aid across Europe).

## 1 | Introduction

The challenge of multi-hazard risk has long been recognised for many natural hazards (Gallina et al. 2016; Hillier 2017; Kappes et al. 2012; UNEP 1992; Ward et al. 2022) and storms in particular (e.g., Southern 1979; White 1974). This co-occurrence of hazards has also recently been framed as ‘compound events’ (e.g., Simpson et al. 2021; Zscheischler et al. 2018). The difficulty is

that the risk of impacts occurring together is harder to quantify, while the impact of a combined event to society can be greater than would be the case if the events were to occur separately (e.g., Hillier et al. 2023).

Inland flooding and extreme winds events cause the largest losses of the weather related hazards affecting North-West Europe (European Environment Agency 2024; Mitchell-Wallace

This is an open access article under the terms of the [Creative Commons Attribution](#) License, which permits use, distribution and reproduction in any medium, provided the original work is properly cited.

© 2025 Crown copyright and The Author(s). *International Journal of Climatology* published by John Wiley & Sons Ltd. This article is published with the permission of the Controller of HMSO and the King's Printer for Scotland.

et al. 2017; PERILS 2024). Illustratively, during 16–21 February 2022 three storms (Dudley, Eunice and Franklin) inflicted various hazards including flooding and extreme winds across the UK and Northwest Europe (Mühr et al. 2022; kendon 2022; Volonté et al. 2024a, 2024b), resulting in multi-sector impacts (e.g., to transport and power distribution) and nearly €4 billion in insured losses (Kendon 2022; PERILS 2023; Saville 2022). Similarly, from 3 to 27 December 1999 the storm sequence of Anatol, Lothar, Martin caused ~€10 billion insured property damage alone in Belgium, Switzerland, Luxembourg, France, Germany and Denmark (PERILS 2024; Roberts et al. 2014).

Strikingly, most of the 98 impactful wintertime (October–March) wind or flood incidents in the PERILS database (PERILS 2024) from 2010 to 2024 affect Great Britain (GB, 73), more than France or Germany (38 or 47, respectively). Moreover, wintertime correlation of proxies for flooding and extreme wind in countries near GB appears similar (Bloomfield et al. 2023; Hillier and Dixon 2020). This is likely because extra-tropical cyclones typically track eastwards from the Atlantic (e.g., Roberts et al. 2014) and are a key driver of both hazards across NW Europe (Figure 1), illustrated by joint wind-flood events during named storms (e.g., Fink et al. 2009; Kendon and McCarthy 2015; Liberato 2014; Matthews et al. 2018). As such GB is a useful sentinel location for studying co-occurring flood-wind impacts in NW Europe.

Building on initial work establishing a relationship between flooding and extreme winds (Hillier et al. 2015; Matthews et al. 2014), there is now strong evidence of co-occurrence in GB on daily to seasonal timescales (Bloomfield et al. 2023; De Luca et al. 2017; Hillier and Dixon 2020; Jones, Stephenson, and Priestley 2024; Martius, Pfahl, and Chevalier 2016; Owen, Catto, Dunstone, et al. 2021; Owen, Catto, Stephenson, et al. 2021), perhaps controlled by the jet stream's characteristics via its influence on cyclogenesis and storm evolution (Hillier and Dixon 2020). Existing work predominantly uses heavy precipitation as a proxy for flooding (e.g., Vignotto, Engelke, and Zscheischler 2021). As reviewed in Bloomfield et al. (2023) studies using observed river flow or impact data, which more directly relate to flooding, are much less common in GB (De Luca et al. 2017; Hillier et al. 2015, 2020) or elsewhere (Küpfer 2024). Indeed, even globally and considering modelled data, work is sparse; only three studies assess the dependency of river flow and wind derived from the same underlying climate model, two in GB (Bloomfield et al. 2023, 2024) and one globally for tropical cyclones (Stalhandske et al. 2024). Thus, future change in joint wintertime flood-wind risk remains of interest.

Two recent studies have used the UK Climate Projections to advance understanding of the drivers of the wintertime co-occurrence of potential flooding and extreme wind in GB, present and future. Bloomfield et al. (2024) used 30 pre-defined weather patterns from the 12 km horizontal resolution regional simulations of this model (hereafter UKCP18r) and a GB hydrological model to assess the meteorological drivers of joint wintertime wind and high flow extremes. For 1-day windows, using population-weighted severity indices, they found cyclonic weather types typical, and also confirmed the positive phase of the North Atlantic Oscillation (NAO+) as an associated

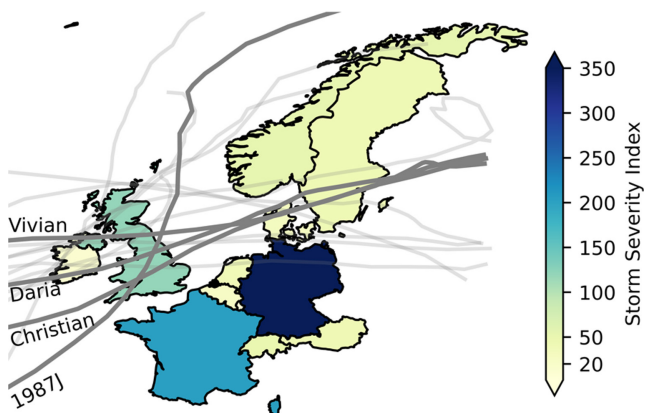


**FIGURE 1** | Indicative map of the distribution of severe wind in NW Europe from a sub-set of 25 storms that caused significant damage in the British Isles from two catalogues (PERILS 2024; Roberts et al. 2014), for which ERA5 data are available (i.e., 1979–2023). Of these, 16 pre-2021 tracks are shown where track data are available (light grey lines) (CCC 2022) with four illustrative tracks labelled and named (dark grey lines). SSI is the Storm Severity index is  $v^3$  over 98th percentile (see Section 2.1) and is a total per country accumulated over the storms. Map projection: Plate carrée. [Colour figure can be viewed at [wileyonlinelibrary.com](http://wileyonlinelibrary.com)]

state (Hillier et al. 2020). At seasonal timescales Bloomfield et al. (2024) also demonstrated a future increase in years that will be both wet and windy (c.  $\times 3$ ,  $p < 0.05$ ). Manning et al. (2024) used the convection permitting UKCP local (2.2 km horizontal resolution) to investigate the role of storm track position and jet stream on the co-occurrence of wind and rain extremes. For individual storm events in mid-winter (December–February) they ascribed future change in co-occurrence to predominantly thermodynamic causes (i.e., warmer and therefore wetter conditions) supported by a more southerly jet stream position during those storms. Both papers find a fourfold increase in short-duration joint events (i.e.,  $\leq 1$ -day) into the future.

Our work here provides several unique contributions to this research area. Using high flows rather than precipitation, it quantifies the co-occurrence of events ( $E$ ) within multi-hazard episodes ( $\epsilon$ ) spanning daily to seasonal durations (i.e.,  $\Delta t = 1$ –180 days long) from October to March in the UKCP18 regional data (1981–1999, 2061–2079). It uses high flows as they do not simply arise from precipitation in individual storms, so the causative storm(s) might differ in character as might antecedent conditions (e.g., soil saturation) and associated jet stream dynamics. It examines more deeply the role of the jet stream, primarily by investigating the role of seasonality (i.e., the time-distribution of events within the winter). To do this it employs an accessible index that is widely used to characterise the latitude and strength of the North Atlantic jet (Woollings, Hannachi, and Hoskins 2010), which will enable future inter-comparison between climate models. Finally, to give real-world relevance it develops an Event Coincidence Analysis approach using dynamically positioned time windows (dwECA) to reflect how these multi-event windy episodes coincident with high river flows ( $\Delta t = 1$ –180 days) are experienced societally.

To define distinct claims (re)insurers commonly use windows of 72 h for storms ( $\Delta t = 3$  days) or 21 days for floods (so-called

'hours clauses' e.g., Mitchell-Wallace et al. 2017; PERILS 2023), which insurers will position to encompass the maximum loss possible. More widely, key impacts are typically documented (e.g., by an emergency response manager) with a day-to-day description e.g., 'It started with the storm on Tuesday, and ended after the last heavy rain on Sunday'. As such, our proposal of dynamic time windows for episodes ( $\epsilon$ ) uses the weather events ( $E$ ) themselves to define the evident start and end of the adverse conditions, as an interested observer might. To study individual weather phenomena (e.g., distinct storm) a buffer approach has been used, such as  $\pm 24$  h (i.e., Manning et al. 2024; Martius, Pfahl, and Chevalier 2016) to give a 3-day symmetrical window. However, it is less straightforward to appropriately capture an episode containing a cluster of storms over a longer period such as 14-days (e.g., Vitolo et al. 2009), and non-overlapping windows or block maxima (e.g., Bloomfield et al. 2023; Zscheischler et al. 2021) may chop a storm in half. Also, time-to-peak modelling of hydrographs indicates that riverine responses to precipitation in GB are  $\lesssim 40$  h (De Luca et al. 2017), giving a lag *after* a storm that should be accounted for. So, as well as aligning with timescales associated with storms, our analysis is designed to align with stakeholder definitions and experience, with insurers providing a specific motivation to focus on time windows ( $\Delta t$ ) of 3 and 21 days. The work has real-world relevance as even in insurance, where natural hazard risk modelling is quite mature (e.g., Mitchell-Wallace et al. 2017) because flooding and extreme wind models of NW Europe are still independently derived; they are based on different underlying climate simulations (Dixon, Souch, and Whitaker 2017; Hillier et al. 2024), with potentially significant underestimates of financial losses (Hillier et al. 2023, 2024).

Using the idea of framing multi-hazard risk environments as an in-depth or user focussed case study to cut through complexity (Hillier and Van Meeteren 2024; Ward et al. 2022) the present work is framed by the insurance sector, yet results are more widely applicable across society, answering four main research questions:

1. To what extent do the most severe extreme winds and flows tend to co-occur? Particularly, asymptotic dependence is considered.
2. How does strength of co-occurrence vary with the time-window ( $\Delta t$ ) used to group events into episodes?
3. How effectively might relatively simple metrics of jet position and strength be used in a functional, readily applied tool to distinguish jet states characteristic of co-occurrence?
4. How do future changes in the North Atlantic jet stream influence co-occurrence in climate model simulations of the future?

## 2 | Data and Methods

The workflow in Figure 2 is used to produce individual events for wind ( $E_W$ ) and flood ( $E_F$ ) with timestamps from the same underlying climate model, namely the UKCP18 12 km, RCP8.5 perturbed parameter ensemble, hereafter UKCP18r. Then,

from these ensemble members, multi-hazard *episodes* ( $\epsilon$ ) are created and analysed. All metrics are calculated during extended winter (October–March) and nationally aggregated. Thresholds are defined from the present-day climate simulations, with values of event severity metrics assigned in absolute terms based on each percentile used, with these 1981–1999 absolute values then applied to future climate to understand potential changes.

Existing data and practice (e.g., thresholds, definitions) are adopted to create events and define their severity (Bloomfield et al. 2023; Griffin, Kay, Bell, et al. 2022; Griffin, Kay, Sayers, et al. 2024; Manning et al. 2024), with a detailed justification of this choice given in Appendix A which updates these discussions to include the latest literature. Importantly, the co-occurrence of events for the simulated present (1981–1999) in UKCP18r replicates well that in historic observations. Respective Spearman's rank correlations between GB aggregated high river flows and extreme wind, calculated for time windows ranging from 1 to 180 days in UKCP18r and observations, match closely. This holds true even when taking multiple historic weather datasets and river-flows derived from them (Bloomfield et al. 2023, 2024; Harrigan et al. 2023; Hersbach et al. 2020; Hirpa et al. 2018). Indeed, these correlations have also been verified against impacts on the GB rail network (Bloomfield et al. 2023). UKCP18r simulations therefore appear to adequately capture the level of co-occurrence between extreme winds and high river flows (detail in Appendix A1).

### 2.1 | Defining Events ( $E$ ) for Each Separate Hazard

Each event ( $E$ ) is a grid of the maxima of a hazard driver (e.g.,  $v$ ) during a time-window containing an isolated hydro-meteorological extreme (detail in Appendix A2). For each event, summary metrics (total area, duration, severity index) are assigned to a single date  $t_{\max}$ , the individual day during the event when the greatest number of grid cells exceeding the set threshold level for that hazard driver. An event's Storm Severity Index,  $SSI(E)$  follows Klapwijk and Ulrich (2003) as given by Equation (1) and Table 1, with this choice of  $SSI$  form and hazard percentile threshold supported by a literature review updated to include the latest work in Appendix A3:

$$SSI(E) = \sum_{i=1}^{N_i} \sum_{j=1}^{N_j} \left( \frac{v(E)_{i,j}}{v_{i,j}^{98}} - 1 \right)^3 \cdot I_{i,j} \quad (1)$$

$$I_{i,j} = \begin{cases} 0 & \text{if } v(E)_{i,j} < v_{i,j}^{98} \\ 1 & \text{otherwise} \end{cases}$$

For simplicity, and to avoid a judgement linking value directly to population density (e.g., consider a wind farm), no population weighting is used. The optimal formulation of  $SSI$  (e.g., power-law, exponential, wind threshold, storm duration) is still actively debated. Most pertinently, probabilistic models that account for the uncertainty in how individual assets are damaged (Heneka et al. 2006; Heneka and Ruck 2008; Pardowitz et al. 2016; Prahl et al. 2012) better approximate losses in Germany across all 2004

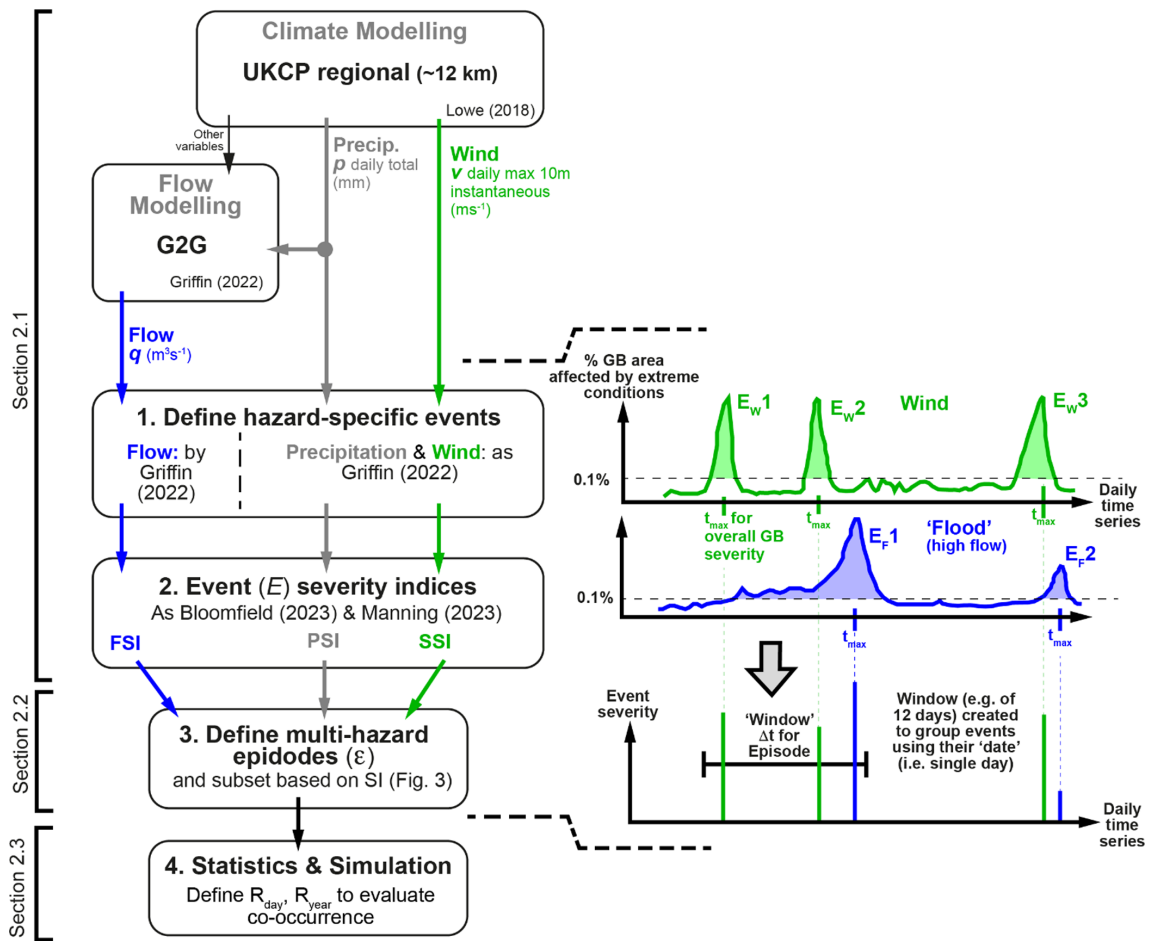


**FIGURE 2** | Workflow used in this analysis, including definitions for some of the variables. Detailed explanation is in main text. For the flow data from Grid-to-Grid (G2G) (Griffin, Kay, Bell, et al. 2022), 0.1% of the river network is ~20 cells, or  $>~20\text{ km}^2$ . For the UKCP18r data on wind gusts and precipitation 0.1% of the GB land area is  $\geq 2$  cells or  $\sim 300\text{ km}^2$ . To find the largest SI to create episodes, FSI and SSI are normalised so that their 95th percentile values are equal (ratio = 1.0). In reality, rare storms might have twice the impact of floods (e.g., Hillier et al. 2024), but sensitivity testing shows that ratios of 0.5 and 2.0 have minimal effect on the episodes defined. Time series are illustrative, not real data. Precipitation is included for completeness (see Appendix A). [Colour figure can be viewed at [wileyonlinelibrary.com](https://wileyonlinelibrary.com)]

**TABLE 1** | Table of parameters used, with precipitation included for completeness (see Appendix A).

| Parameter  | Symbol                             | Units                     |
|--|------------------------------------|---------------------------|
| Maximum daily 10 m wind gusts at a grid cell $i,j$ , and the threshold (98th) percentile taken to define extreme at a grid cell  | $v, v_{i,j}, v^{98}$               | $\text{ms}^{-1}$          |
| Total daily precipitation, and the threshold (98th) percentile taken to define extreme at a grid cell  | $p, p_{i,j}, p^{98}$               | $\text{mm}$               |
| Daily mean river flow  | $q, q_{i,j}, q^{99.5}$             | $\text{m}^3\text{s}^{-1}$ |
| Day  | $t$                                | Days                      |
| Event $E$ . Type of event is $W, F$ or $P$ : $W$ is for Wind, $F$ is for river flows and $P$ is precipitation. $k$ is the event's identification number within the set   | $E_{W,k}$                          | —                         |
| Multi-hazard episode $\epsilon$ , with its type (wind $W$ , high flow $F$ , joint $J$ ) and severity percentile exceeded by the episode's constituent events (i.e., > 75th, 95th or 99th of events within the relevant event set). Also see Figure 3 | $\epsilon_W^{95}$                  | —                         |
| Event's most extreme day, to which summary statistics (e.g., duration, FSI) are assigned   | $t_{\max}$                         | Days                      |
| Temporal limits of an event (i.e., start and end)  | $t_{\text{start}}, t_{\text{end}}$ | Days                      |
| Length of multi-hazard episode, 'time window'  | $\Delta t$                         | Days                      |

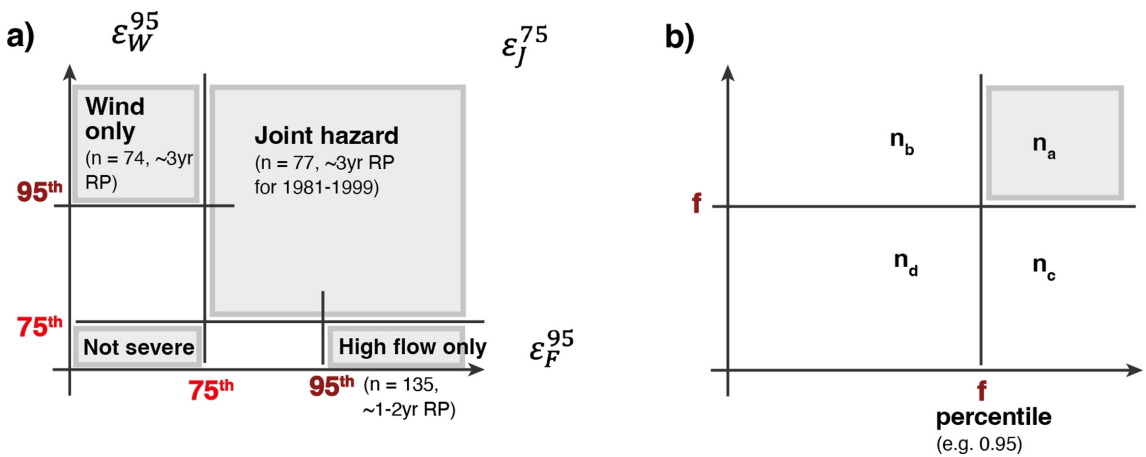


**FIGURE 3** | (a) Illustration of subsets and nomenclature used, with numerical detail for  $\Delta t = 3$  during 1981–1999 from Figure 4a.  $\varepsilon_J^{75}$  is the subset of all episodes with both hazards jointly having at least one event exceeding the 75th percentile. Also see Table 1. (b) Nomenclature used to define  $U$  in Section 2.3:  $F$  is the percentile threshold defining episodes as large or potentially impactful, as a fraction;  $n$  is the total count of episodes, divided into subsets  $n_a$  to  $n_d$  depending upon whether or not they exceed the threshold for river flow on the  $x$ -axis and/or extreme wind on the  $y$ -axis. [Colour figure can be viewed at [wileyonlinelibrary.com](http://wileyonlinelibrary.com)]

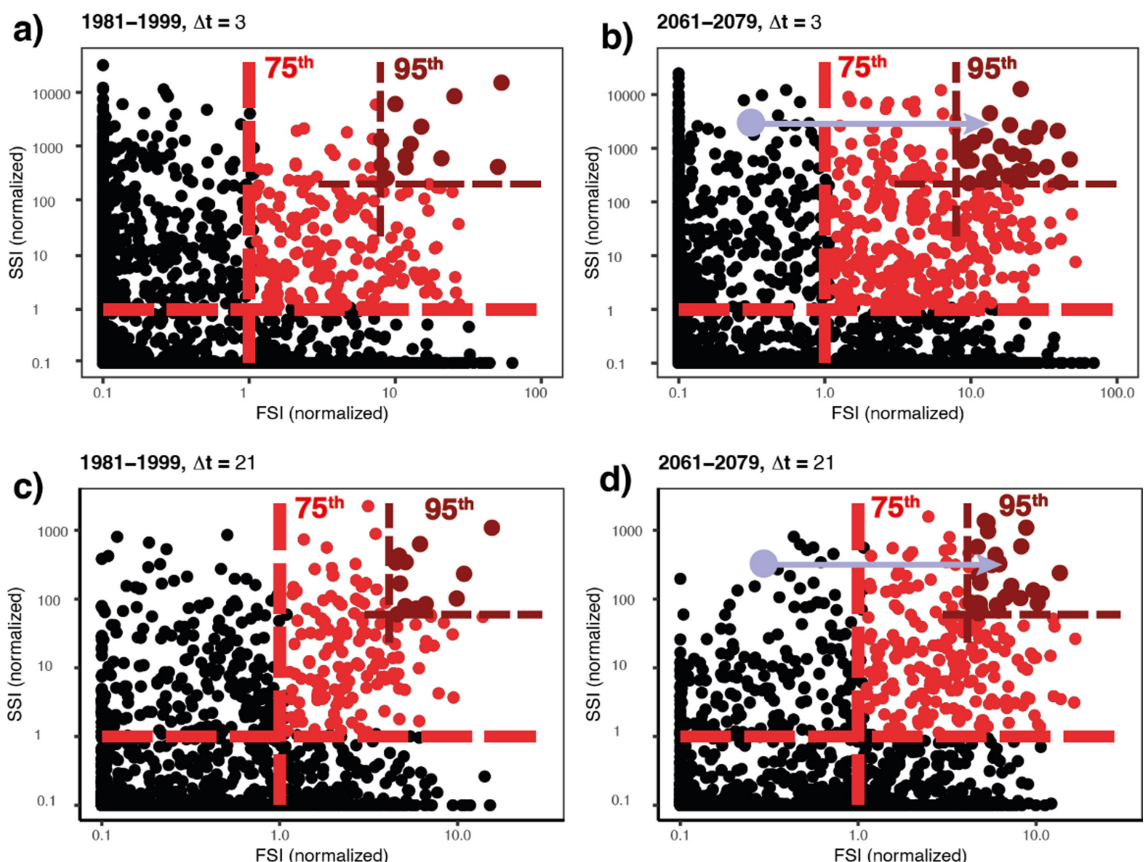


**FIGURE 4** | Scatter plots of the summed severity of potential flooding (FSI) and extreme wind (SSI) for 3-day episodes for (a) present and (b) future time slices relative to the 75th percentile of these measures. Two thresholds are shown, the 75th percentile (red) and 95th percentile (dark red). Thresholds for 1981–1999 are used in all panels. (c) and (d) are the same, but for 21-day episodes. Light blue arrows visually highlight the tendency for FSI to increase into the future, which is particularly prominent for  $\Delta t = 21$ . [Colour figure can be viewed at [wileyonlinelibrary.com](http://wileyonlinelibrary.com)]

wintertime days in 11 years (1997–2007). The exception to this is the costliest days (~10 per year), which are still adequately modelled using cubic excess-over-threshold approach with a 98th percentile (Prahl et al. 2015). Thus, using Equation (1) is appropriate here. Because recent developments have not been previously

reviewed, a detailed justification is in Appendix A3. The new wind event set is described in Appendix A4.

Based on the form of SSI, Flood Severity Indices (FSI) have recently been developed (Bloomfield et al. 2023). Only grid cells on

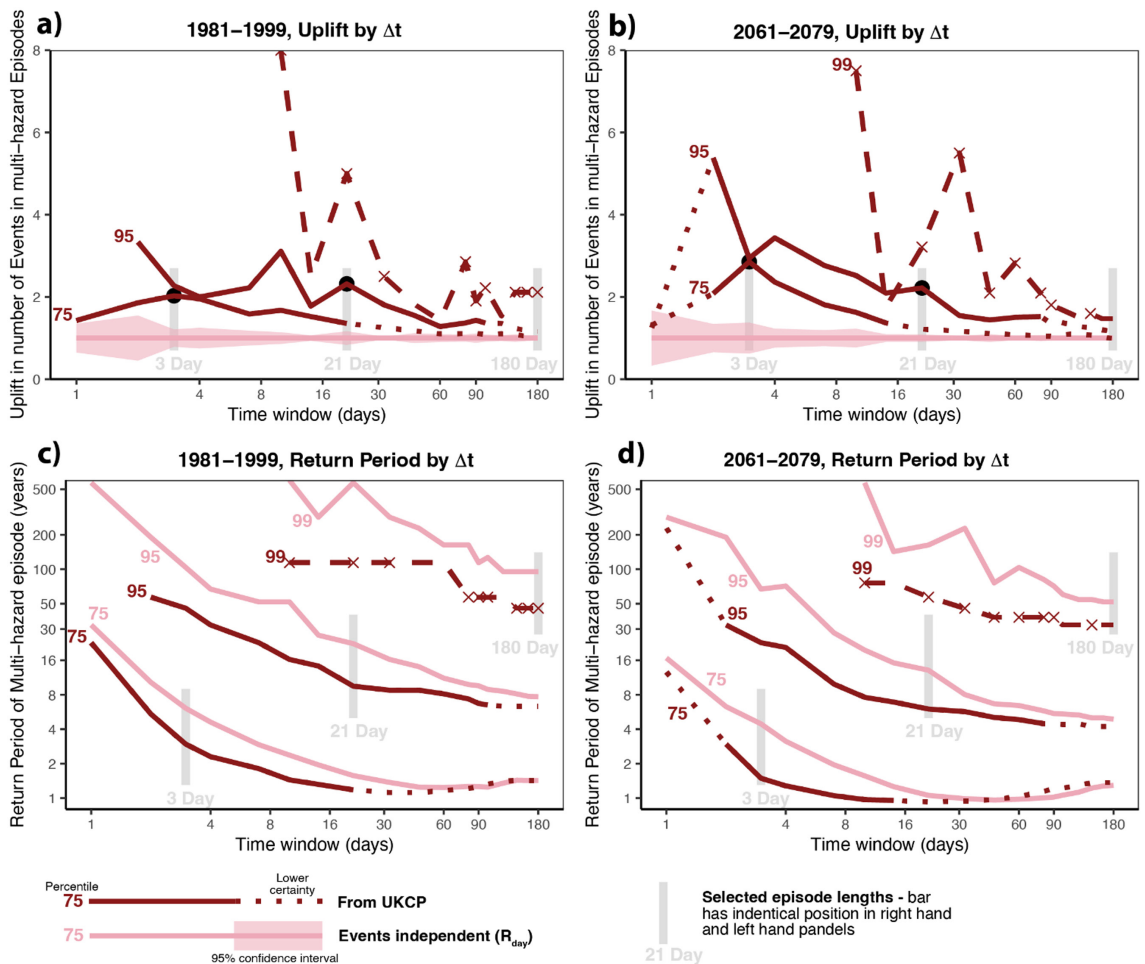


**FIGURE 5** | Enhancement in co-occurrence, for a range of window lengths ( $\Delta t$ ) used to create episodes. (a) Uplift in number of events involved in multi-hazard episodes (1981–1999) as compared to a baseline of independence (pink line,  $R_{\text{day}}$ ). Solid red lines are statistically significant, unlikely from variability within the independent case (pink shading is  $2\sigma$ ) assessed by simulation. Joint episodes  $\epsilon_j^{75}$  are labelled '75', and so on. The Black dots situate the analyses of Figure 6 within this plot. Dashed line indicates lower subjective confidence as occurrences get low, with 'x' marking statistically significant points. Dotted lines on Figure 5 indicate that caution is needed, where episodes occupy  $> 10\%$  of time because 'remnant' time periods left between already created episodes might start to appear, or where the observation is not clearly different from the baseline (i.e.,  $p > 0.05$ ) because  $n$  becomes low or the difference small. (c) and (d) Return period of multi-hazard episodes at 3 percentiles (75, 95 and 99). Note that the grey bars are identically positioned on (a) and (b), and on (c) and (d). [Colour figure can be viewed at [wileyonlinelibrary.com](http://wileyonlinelibrary.com)]

the river network are used, again with no population weighting. Thus, each events' flood severity  $\text{FSI}(E)$  is given by Equation (2) and Table 1 with the 99.5th percentile choice based on previous sensitivity testing and verifications (Bloomfield et al. 2023; Griffin, Kay, Bell, et al. 2022; Griffin, Kay, Sayers, et al. 2024); see Appendix A2 for a detailed justification.

$$\text{FSI}(E) = \sum_{i=1}^{N_i} \sum_{j=1}^{N_j} \left( \frac{q(E)_{i,j}}{q_{i,j}^{99.5}} - 1 \right) \cdot I_{i,j} \quad (2)$$

$$I_{i,j} = \begin{cases} 0 & \text{if } q(E)_{i,j} < q_{i,j}^{99.5} \\ 1 & \text{otherwise} \end{cases}$$

Debate on the form of FSI is expected to continue, so a detailed justification is in Appendix A3. Pertinently, FSI as configured in Equation (2) is suitable here as only extreme and potentially damaging events are later selected for analysis,

namely those exceeding at least the 75th percentile of events (see Figure 3); using the 75th percentile for this selection gives 5–6 high flows per year, comparable to the ~7 floods per year in commercial risk models (Hillier et al. 2024). The threshold used depends on the time window  $\Delta t$  as explained below, and sensitivity testing has been conducted to examine the impact of these choices (Figure 5).

## 2.2 | Defining Multi-Hazard Episodes ( $\epsilon$ )

Extratropical cyclones cluster in time, with two or three meteorologically distinct cyclonic systems (Mailier et al. 2006; Vitolo et al. 2009) combining in longer windy periods. Similarly, rainy days occurring in succession might be grouped in episodes (Kopp et al. 2021). Here, this concept is applied to multi-hazards (Figure 2), adopting the term *episode* ( $\epsilon$ ) and applying it to mean a grouping in time of hazardous events ( $E$ ) within a selected spatial domain as is established practice when hazards co-occur (e.g., Bloomfield et al. 2023; De Luca et al. 2017; Hewitt and Burton 1971;

Hillier et al. 2015; Kappes et al. 2012). In this case, the domain is set to GB. The temporal grouping approach accounts for a time-lag between events as do Claassen et al. (2023), but the protocols differ in that here they are stakeholder rather than hazard driven. In particular the time-lag here might also be due to impact related factors (e.g., time to develop, repair or recovery time, staff fatigue, an organisation's reporting timeframe, an April–March financial year) not just duration and overlap of physical hazard (e.g., Hillier et al. 2023; Hillier and Dixon 2020; de Ruiter et al. 2019).

Episodes are defined for a prescribed window length of  $\Delta t$  days, although the episode creation process can be repeated later for other window lengths. For each  $\Delta t$ , episodes are defined by starting with the event with the greatest severity index (SI), placing a window of length  $\Delta t$  days around it dynamically positioned so as to capture other events that create the largest total SI (see Figure 2), and then removing these events from the initial list. Then, this is repeated until all events are accounted for. Once created, an episodes' severity at this  $\Delta t$  must be quantified.

That flood-wind co-occurrence might be enhanced by a greater frequency of an NAO+ state across a 180-day season (Bloomfield et al. 2024; Hillier et al. 2020) raises the technical question of how to quantify severity for long episodes. This depends on stakeholder and purpose. It is possible to simply sum daily SSI or FSI (Bloomfield et al. 2023), implicitly assuming that each day is independent and additive in its impact (i.e., duration/persistence is significant). Is being flooded at 2.0 m depth for 5 days five times more damaging than for 1 day? For an electricity network operator fined by customer minutes lost, it might be (Wilkinson et al. 2022). As the strongest gusts or highest river levels during an event approximate insured damage well (Mitchell-Wallace et al. 2017), an alternative is to use an event-based approach (e.g., Griffin, Kay, Sayers, et al. 2024; Roberts et al. 2014), then sum events' losses. This implicitly assumes a reset between events, ignoring duration (Appendix A3) and is the (re)insurance approach followed in Figure 4.

Here, our main aim is to quantify the co-occurrence of large events that drive risk. So, episodes ( $\epsilon$ ) are classified by the severity of their constituent events (Table 1), with thresholds chosen to select potentially impactful events (Section 2.1, Appendix A3) and mutually exclusive subsets containing roughly equal numbers of episodes (i.e., RPs). This classification is *not* a summation. Illustratively,  $\epsilon_W^{95}$  contains at least one wind event  $E_W$  with an SSI in the top 5% of wind events but no high flow event. Figure 3 shows the thresholds for  $\Delta t = 3$  days. For  $\Delta t = 21$  days, since longer windows can more readily unite rarer and more extreme events, joint hazard ( $\epsilon_J$ ) uses the 95th percentile and individual hazards ( $\epsilon_F, \epsilon_W$ ) the 99th.

### 2.3 | Statistical Simulation for Co-Occurrence Analysis

A variety of options exist to quantify dependency of hydro-meteorological extremes (e.g., Bevacqua et al. 2021; Heffernan and Tawn 2004; Serinaldi and Papalexiou 2020), although it is advised to ensure that they are not reinvented or untested (Serinaldi, Lombardo, and Kilsby 2022). One well-established approach is

using copulas to fit a distribution to data extreme in both variables (e.g., Bevacqua et al. 2017; Manning et al. 2024). This permits smoothed curves to be fitted, but relies upon selecting an appropriate distribution (e.g., Gumbel copula). Alternatively, extremal dependency for wet and windy conditions can be quantified by measures of the co-occurrence of extremes above a given percentile (Hillier et al. 2015; Martius, Pfahl, and Chevalier 2016; Owen, Catto, Stephenson, et al. 2021).  $\chi$  (Coles, Heffernan, and Tawn 1999) and uplift in co-occurrence  $U$  (De Luca et al. 2017; Hillier et al. 2015), which are closely related (Equations (3) and (4))- with nomenclature as defined in Figure 3b.

$$\chi = \frac{n_a}{(1-f)n} \quad (3)$$

$$U = \frac{n_a}{E[n_a]} = \frac{n_a}{(1-f)^2 n} \quad (4)$$

$\chi$  is the probability that one variable is extreme if the other is also extreme, varying between 0 and 1 (e.g., Bloomfield et al. 2023; Vignotto, Engelke, and Zscheischler 2021).  $U$  is an occurrence ratio, the observed number of co-occurrences divided by the number expected due to chance for independent events (i.e.,  $E[n_a]$ ). It is also, therefore, the extent to which one would underestimate the probability of co-occurrence if independence were assumed. Some authors have called  $U$  a 'Likelihood multiplication factor' (Ridder et al. 2020; Zscheischler and Seneviratne 2017). With independent events uniformly distributed over a time period, the significance of  $U$  is found with a binomial test (Bevacqua et al. 2021), but  $E[n_a]$  can also be simulated directly.

Event coincidence analysis (ECA) is a method in time-series analysis to assess if one type of event might be a precursor to another based on an underlying Poisson process (e.g., netCoin or CoinCalc R packages) (Donges et al. 2016; Escobar 2015; Siegmund, Siegmund, and Donner 2017). With the dynamic positioning of the window and  $1-n$  events potentially within each episode, it is not straightforward to construct this analytically. So, statistical simulation modelling (e.g., Hillier et al. 2015; Ridder et al. 2020) is used to calculate  $E[n_a]$  to investigate  $U$  in UKCP18r by eliminating elements of its temporal structure (Hillier et al. 2015, 2020; Hillier and Dixon 2020; Zscheischler et al. 2021). For this simulation modelling an ECA is designed that uses dynamic windows to form episodes, which we name here dwECA; in conjunction with this two simpler (i.e., less structured) models of events are created, from which episodes are then formed as in Section 2.2 for comparison with the episodes directly extracted from UKCP18r.

1. Model  $R_{\text{day}}$ : For each event, year and day are randomised, a uniform distribution. This is  $E[n_a]$ , reflecting an October–March climatology approach (e.g., Champion, Allan, and Lavers 2015; Smith and Phillips 2012; Stephan, Ng, and Klingaman 2018), or a business-as-usual case in (re)insurance (e.g., Hadzilicos et al. 2021; Hillier et al. 2024).
2. Model  $R_{\text{year}}$ : For each event, only year is randomised. All relationships to proximal events within a time-series are broken up to and including inter-seasonal timescales, yet seasonality (i.e., the pattern of frequency as time progresses

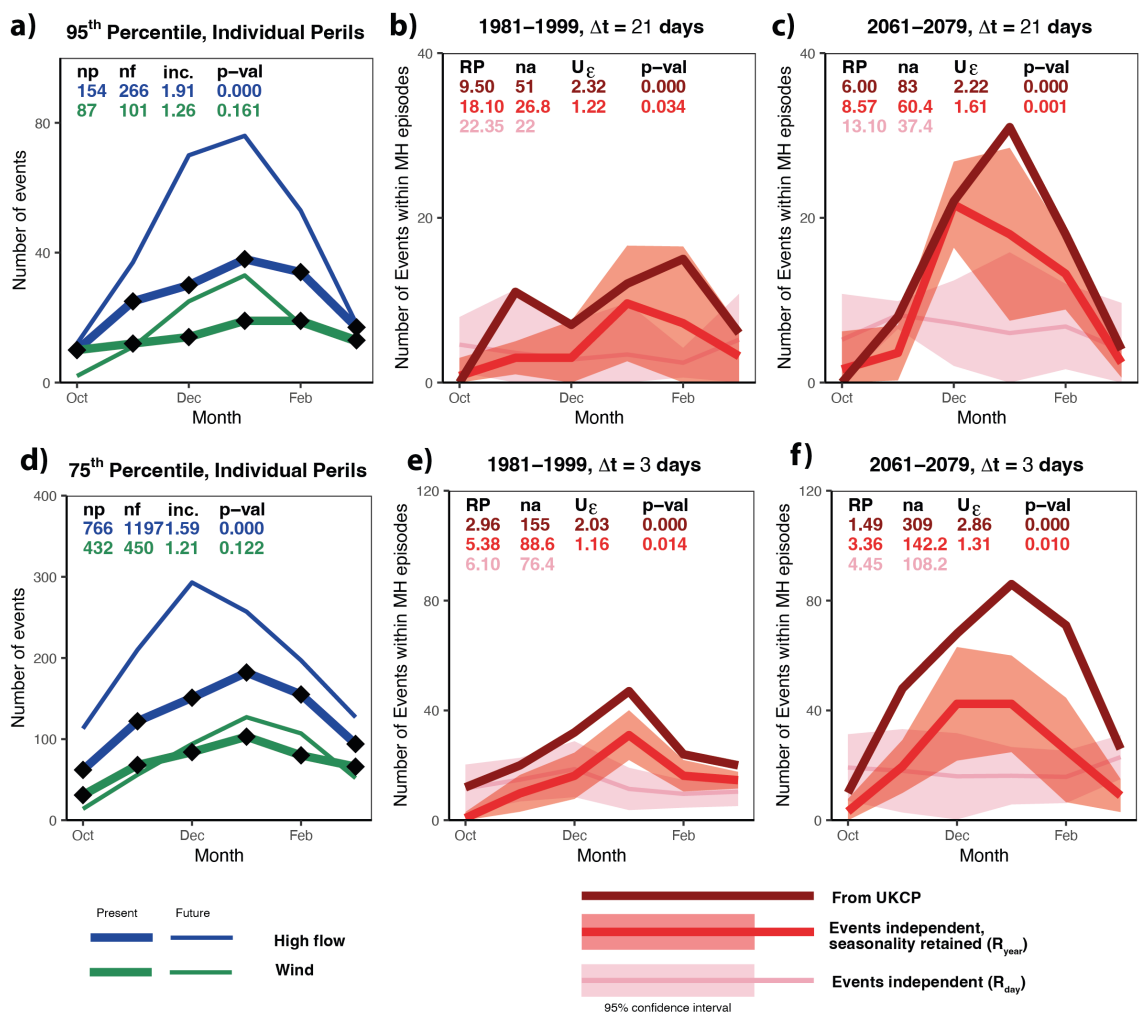


**FIGURE 6** | Seasonality of individual events ( $E$ ) and multi-hazard episodes ( $\epsilon$ ). (a) Seasonality of events for all high-flows (blue) and extreme wind (green) exceeding the 95th percentile. Thick lines represent 1981–1999 and thin lines 2061–2079.  $n_p$  and  $n_f$  are total counts for the present and future, respectively. ‘inc.’ is the mean increase (multiplier) from present to future for the 12 ensemble members with the  $p$  value for the total count assessed using their variability ( $t$ -test). (b) and (c) Number of events in multi-hazard episodes  $\epsilon^{95}$  from UKCP18r (dark red), simulations with dependency broken but retaining seasonality (red,  $R_{\text{year}}$  model), and independent phenomena (pink,  $R_{\text{day}}$  model). Coloured ribbons are  $2\sigma$ , assessed by simulation. RP is return period of episodes in years, and  $p$  values are calculated using variability of statistical model runs  $R_{\text{day}}$  and  $R_{\text{year}}$  ( $t$ -test). (c) as for (b) except for the future climate period. (d)–(f) as for (a)–(c), but for the 75th percentile and  $\Delta t = 3$ . [Colour figure can be viewed at [wileyonlinelibrary.com](http://wileyonlinelibrary.com)]

through a winter) is retained. This avoids pre-supposing a December–February peak storm season (e.g., Manning et al. 2024; Martius, Pfahl, and Chevalier 2016), as this may change in future.

Episodes created from events directly extracted from UKCP18r contain real-world dependencies (e.g., storms triggering both wind damage and flooding), while dependencies do not exist in models  $R_{\text{day}}$  and  $R_{\text{year}}$ . Thus, the difference between co-occurrence in modelled worlds with and without dependency (i.e.,  $U$ , Equation (4)) reveals the effect on co-occurrence of those dependencies; that is, models  $R_{\text{day}}$  and  $R_{\text{year}}$  are directly equivalent to a null hypothesis, what could happen only by chance, the basis of all inferential statistics. The relative sizes of uplift  $U$  for different window lengths (e.g.,  $\Delta t = 3, 21$  days) allows insight into phenomena that act on different timescales (e.g., storms, or clusters of storms). A key advantage of this simulation approach is its simplicity. Designing a statistical model to replicate observations

requires the multiple choices in the selection of statistical distributions and parameters, but there are no such choices here.

Note that all randomisation is conducted separately within each ensemble member. This is cautious (i.e., perhaps less significant  $p$  values) but remains valid even if the 12 ensemble members of UKCP18r are not a truly random sample. Randomisation is repeated five times, giving 1140 simulated years in total, 228 for each statistical model run. The chance ( $p$  value) of occurrences in UKCP18r occurring in the simplified models can then be assessed by taking each as a null hypothesis  $H_0$  (i.e., Figures 5 and 6). Here, for episodes, uplift  $U_{\epsilon}$  is the total count of the number of events ( $n_a$ ) over threshold within episodes.

## 2.4 | Jet Stream Metrics

One widely used and relatively simple metric of jet position is that of Woollings, Hannachi, and Hoskins 2010. This diagnostic uses

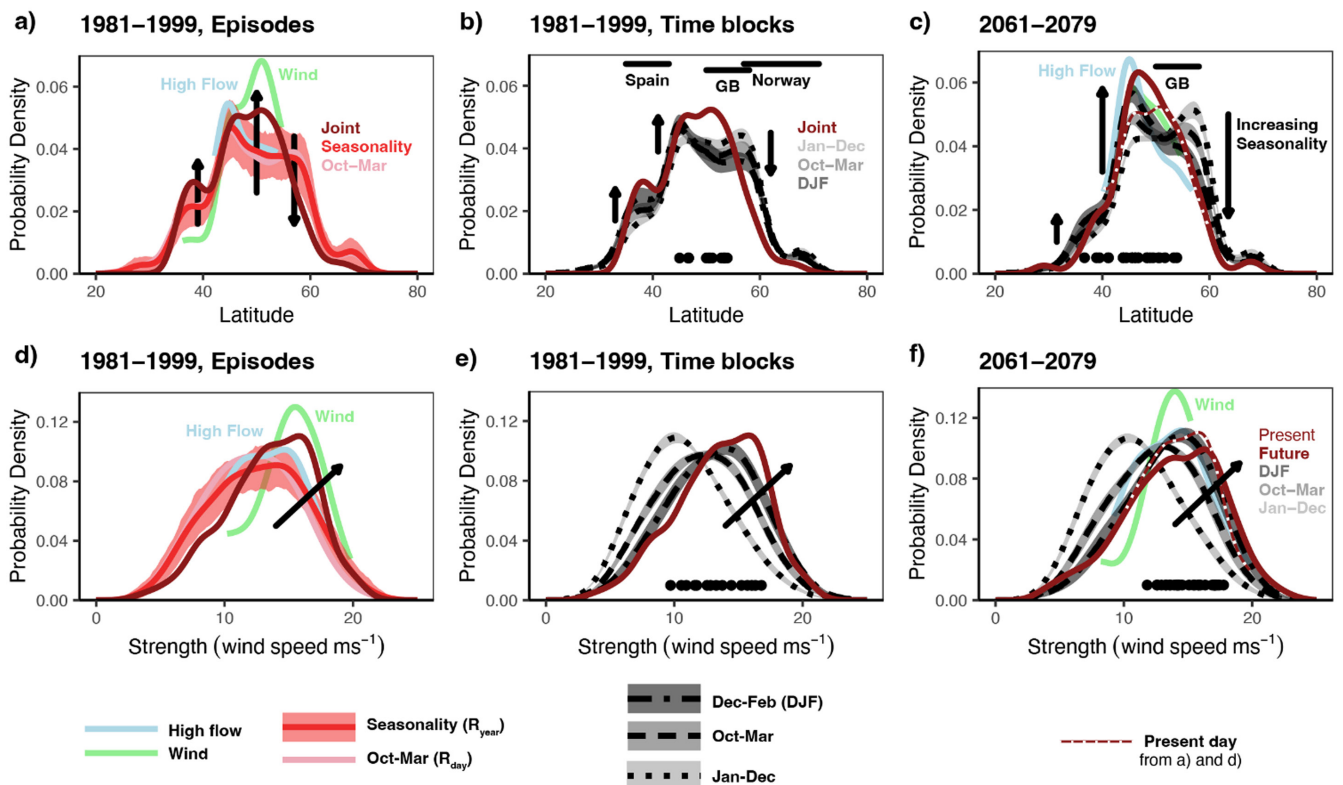


**FIGURE 7** | Jet latitude (top row) and strength (bottom row) in UKCP18r (McSweeney and Bett 2020) associated with  $\Delta t = 3$  joint high flow and extreme wind episodes ( $\epsilon_J^{75}$ ), present and future. Curves are density estimates (Gaussian kernel,  $\sigma = 1.0$  for strength and  $\sigma = 2.0$  for latitude), and arrows illustrate trends identified in the data. In panels (a) and (d), the light red line is sampling preserving the distribution of storms' dates within a season (i.e.,  $R_{\text{year}}$ ) and the pink lines are for October–March (i.e.,  $R_{\text{day}}$ ) and the error ribbon is 10th–90th quantiles for these storms as estimated from 100 random realisations. Uncertainty for the selected seasons (b, c, e, and f) is shown as grey shading and is  $\pm 2\sigma$  stderr of the 12 ensembles of UKCP18r. For visual clarity, only the parts of the wind and high-flow curves ( $\epsilon_W^{95}, \epsilon_F^{95}$ ) are shown where they differ notably from the other curves. Dots are the most extreme events ( $\epsilon_J^{95}$ ). Bars in (b) and (d) show the latitude ranges of illustrative countries. All days within each episode are used. [Colour figure can be viewed at [wileyonlinelibrary.com](https://wileyonlinelibrary.com)]

four low-level wind fields (925–700 hPa) to quantify the latitude and speed of the eddy-driven jet stream. It is zonally averaged over the North Atlantic (0–60° W, 15–75° N), low pass filtered with a 10-day window to remove effects from individual synoptic systems, then the maximum westerly wind speed across the latitudes is taken to locate and quantify the jet. Data used here (McSweeney and Bett 2020) are taken from the UKCP18 global model, which drives the regional model used in this paper.

### 3 | Results

Visually, on Figure 4, a first impression is that the number of more severe joint episodes ( $\epsilon_J$ ) increases in a future climate. This is investigated further for a range of time periods and thresholds (Section 3.1). Then, distribution by month or ‘seasonality’ is explored (Section 3.2). Finally, the jet stream is examined as a possible cause of the observed patterns (Section 3.3).

#### 3.1 | Uplift Factors

Uplift ( $U_\epsilon$ ) is the number of times more common co-occurrences are in UKCP18r than expected for independent events uniformly

distributed across October–March (i.e.,  $R_{\text{day}}$ , pink). Figure 5a clearly shows two patterns (red lines) for the present.

1.  $U_\epsilon$  is broadly two to four for all  $\Delta t$  (1–180 days) and percentiles (75–99th), but difficult to detect for seasonal timescales.
2.  $U_\epsilon$  is highest for more extreme events (i.e., rarer, larger percentiles) and at shorter time windows (i.e., smaller  $\Delta t$ ).

Visually,  $U_\epsilon$  is similar in future (Figure 5b), best seen by comparison to the grey vertical lines which are identical in each panel. As  $U_\epsilon$  is relative to a baseline ( $R_{\text{day}}, E[n_a]$ ) that accounts for the total of severe events (i.e.,  $n_a + n_b + n_c$ , see Figure 3b) increasing in future, it isolates the potential change in the dependence structure (i.e., level of ‘correlation’). Illustratively, for  $\Delta t = 3$  at the 95th percentile in 2061–2079 ( $\epsilon_J^{95}$ ), the UKCP extract that includes dependence has a 23-year return period (red line, Figure 5d), which is considerably lower than the 104-year value for the simulation that enforces an assumption of independence (pink line). Return periods (RPs) in Figure 5c,d are simply calculated based on the number of episodes ( $n_\epsilon$ ) that exceed a severity threshold for a given  $\Delta t$  (i.e.,  $RP = \text{years}/n_\epsilon$ ). As such, the increased number of high-flow events is reflected in RPs reduced to about half their present value.

For 1-day windows, the act of collapsing events to a single day ( $t_{\max}$ ) will tend to underestimate co-occurrence, as flooding is expected to peak the day after wind given that water takes time (typically up to 24 h) to flow into and through GB's rivers (De Luca et al. 2017); daily or storm-based analyses (Bloomfield et al. 2023; Manning et al. 2024) will be less influenced in this particular.

### 3.2 | Seasonality

Distribution by month of the co-occurrence of severe episodes, their seasonality, is explored in Figure 6 at the key timescales of  $\Delta t = 3$  and 21 days using  $\epsilon_J^{75}$  and  $\epsilon_J^{95}$ , respectively. Since a longer window is more likely to contain extreme events, a higher threshold captures sufficient events for  $\Delta t = 21$ . There are three pertinent features:

1. Considered individually (Figure 6a,d), both high flows and wind are notably more seasonal in future, more concentrated in midwinter (December–February); the exception is lower (75th) percentile flows. This effect is greater for the higher (95th) percentile (Appendix B).
2.  $U_e$  is 2–3, present and future, aligning with Figure 5.
3. For  $\Delta t = 21$ , the red line ( $R_{\text{year}}$ ) is only a little below the UKCP18r occurrences (dark red), so at a storm-sequence timescale of weeks ( $\Delta t = 21$ )  $U$  can largely be modelled by seasonality (i.e.,  $R_{\text{year}}$ ); the small but significant difference in January and February in future is worth noting for investigation in further research. However, on a shorter timescale ( $\Delta t = 3$ ), an additional physical mechanism must be invoked that operates on a shorter time-scale, that of a single storm or storms in fairly rapid sequence (i.e.,  $\Delta t \sim 2$ –10 days).

Note that the seasonality effect in this bootstrap modelling ( $R_{\text{year}}$ , Figure 6c) arises simply due to more events being placed (e.g., by a broader-scale atmospheric driver) in a restricted time-frame. Illustratively, consider a daily analysis of 10 winters each comprising 100 days, containing 50 floods and 50 wind extremes in total. If uniformly distributed (i.e., Poisson randomness), the expected number of co-occurrences is  $0.05 \times 0.05 \times 1000 = 2.5$  coincidences (e.g., Bevacqua et al. 2021; Hillier et al. 2015). Now, compress these into the central 50 days, the expectation is  $0.1 \times 0.1 \times 500 = 5.0$  coincidences.

### 3.3 | Jet Stream

Figure 7 investigates the jet stream as a potential physical mechanism for the uplift  $U$  that cannot be explained by seasonality for 3-day episodes ( $\epsilon_J^{75}$ ) identified in Section 3.2. Jet characteristics for the days of these episodes are plotted, with other subsets ( $\epsilon_F^{95}, \epsilon_W^{95}$ ) (see Figure 3a) and average values for time blocks (e.g., December–February) displayed for comparison. Figure 8 presents a differently derived view, maps of westerly wind velocity anomalies on  $t_{\max}$  days. Exact consistency between the two is not expected.

A number of features support the reliability and relevance of the main results to follow. First, in Figure 7 subsets (e.g.,  $\epsilon_J^{75}, \epsilon_W^{95}$ ) are distinct from time blocks and the statistical models

( $R_{\text{year}}, R_{\text{day}}$ ). This simply would not happen if there were a mismatch (e.g., in timing) between the metrics of the jet in the global model (McSweeney and Bett 2020) and extreme weather extracted here for GB from the regional model. Second, the present day trimodal peak in ERA-40/ERA-Interim, matched 'reasonably well' by UKCP18r (McSweeney and Bett 2020; Woollings, Hannachi, and Hoskins 2010), is present (Figure 7a,b). Third, on days that severe weather occurs in GB jet-related wind anomalies occur over NW Europe, not elsewhere (Figure 8), indicating that the jet metrics (McSweeney and Bett 2020; Woollings, Hannachi, and Hoskins 2010) are relevant to the study area.

For 1981–1999 joint severe episodes' ( $\epsilon_J^{75}$ , dark red line) jet strength and latitude differ discernibly from conditions at the times of year that they typically occur (i.e.,  $R_{\text{day}}$ , red line and shading in Figure 7) and from average October–March conditions ( $R_{\text{day}}$ ); October–March curves match those for non-severe storms ( $\epsilon_J^{<75}$ ) very closely, although these are not shown for visual clarity (Figure 7). Extremes also differ from a jet typical of the mid-winter DJF storm season. Specifically, the four differences are:

1. Days with only high flows ( $\epsilon_F^{95}$ ) have jet latitude frequency peaks at 45°N, marginally elevated above the seasonal expectation (Figure 7a). Similar is true for jet strengths (Figures 7d and 8b).
2. Potentially damaging winds in isolation ( $\epsilon_W^{95}$ ) are associated with a strong jet typically focussed on 45–55° latitude range (Figure 7a,d) with a jet speed anomaly at relatively high latitudes (50–60°N) extending across the Atlantic (Figure 8a).
3. Jet latitude for joint  $\epsilon_J^{75}$  episodes peaks distinctly at 50°N (Figures 7a,d and 8c). Self-evidently this is largely due to GB's latitude (Figure 7b) because storms used here must impact GB, and the southwards displacement in this subset is highlighted with vertical arrows (Figure 7a).
4. The peak in  $\epsilon_J^{75}$  jet latitude is between the  $\epsilon_F^{95}$  and  $\epsilon_W^{95}$  peaks (Figure 7a), and their jet strength is intermediate in a progression from the high-flow to wind curves (Figure 7d, arrow). In map view, the joint  $\epsilon_J^{75}$  anomaly is also a blend of those from the individual hazards (Figure 8a–c). A southerly lobe extending into the mid-Atlantic (20–40°W) is also notable.

Overall, co-occurring events in 1981–1999 appear to be associated with a jet that blends characteristics of the most severe high-flow inducing events (i.e., similar to expectations for the time of year) with the severest wind events. This is true even for the most severe episodes (i.e.,  $\epsilon_J^{95}$  shown as black dots,  $n = 5$  with a RP of 44.8 years).

How does the jet strengths and latitudes change for 2061–2079? Broadly, most patterns are similar in their character to 1981–1999, but with some important changes in relative magnitudes. The main changes are:

1. In future, jet strength and latitude anomalies ( $\epsilon_J^{75}, \epsilon_W^{95}, \epsilon_F^{95}$ ) are of higher amplitude with respect to 1981–1999 (Figures 7 and 8), insensitive to the exact baseline chosen (e.g.,  $R_{\text{year}}$ , non-severe).
2. For jet latitude, the peak for joint extremes ( $\epsilon_J^{75}$ ) shifts ~3° southwards, as do the conditions for the individual hazards,

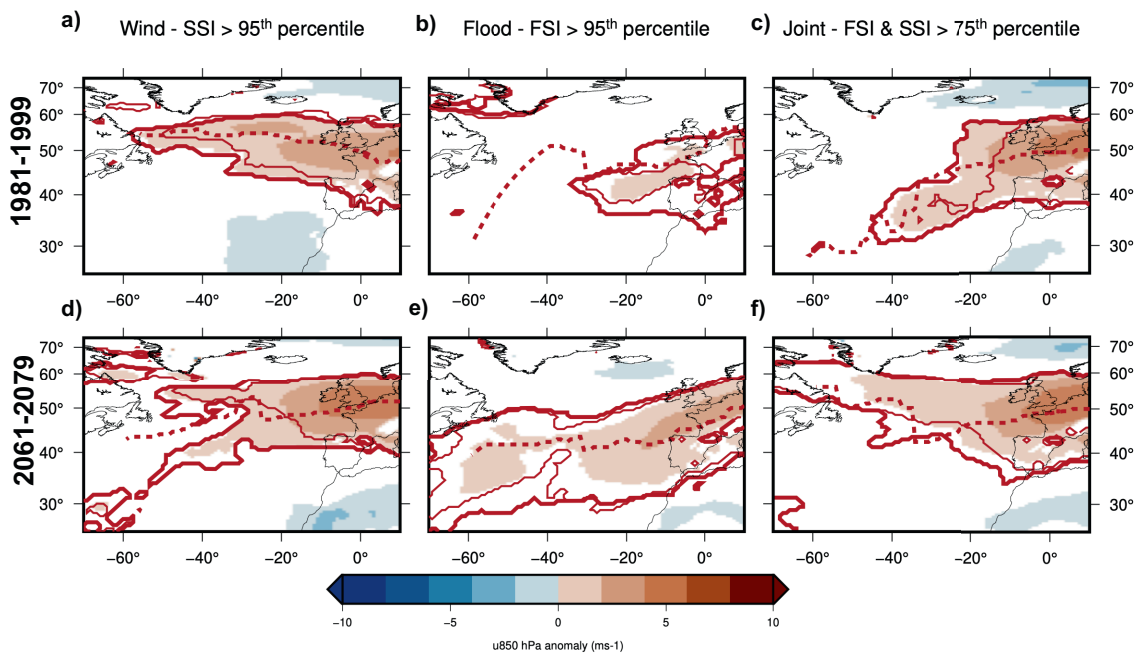


**FIGURE 8** | Plan view of eddy-driven jet anomalies during stormy episodes ( $\Delta t = 3$ ) in comparison to the October–March climatology. Composites of daily mean zonal wind velocity at 850 hPa for (a) dates of wind extremes ( $\epsilon_W^{95}, n = 74$ ), (b) high-flow extremes ( $\epsilon_F^{95}, n = 135$ ), and (c) days where both are extreme ( $\epsilon_J^{75}, n = 77$ ). (a)–(c) are for 1981–1999, and (d)–(f) are for a future climate. Days used are only the most severe day within an episode (i.e.,  $t_{\max}$ ). Solid red lines outline areas where the positive anomaly is significant ( $p < 0.05$ ) for one-tailed  $t$  test for difference between means of 12 ensemble members (climatology) and severe episodes. For comparison, thin red outlines are for a DJF climatology, and dashed line is the most significant point at each longitude for a higher-level jet (u250). Hobo-Dyer (i.e.,  $37.5^\circ$  standard parallel) cylindrical equal area projection, with  $-30^\circ$  meridian. Note that (f) is reconciled with Figure 7c by realising that those data ( $u$  maximum) typically occur near NW Europe. [Colour figure can be viewed at [wileyonlinelibrary.com](http://wileyonlinelibrary.com)]

perhaps caused by the enhanced future seasonality of the jet which shifts southwards in midwinter despite an overall (January–December) shift northwards (Figure 7c).

3. Future DJF jet strength is similar to the present-day jet states for joint storms (Figure 7f).
4. In map view (Figure 8) anomalies for future wind episodes remain in a similar location, those for high flows expand south and west, and the anomaly for joint hazards like in 1981–1999 shares characteristics with both; in Europe it extends to Iberia like for high-flows, but across the Atlantic at  $50$ – $60^\circ$  N like wind. This is a switch from a high-flow like pattern to a wind-like one (see Section 4.4).

In short, mean future DJF jet conditions tend to adopt a latitude that characterises high-flows in GB today and a jet strength typical of joint extremes today (Figure 7c,f). Thus, in future, typical shorter-term ( $\Delta t \lesssim 10$  days) midwinter jet states appear like those characteristic of impactful compound storms today, aligning with the observation that  $\epsilon_J^{75}$  become more focussed in DJF (Figure 6). The most severe episodes ( $\epsilon_J^{95}$ ) reflect this, being twice as frequent with a somewhat stronger and more southerly jet (i.e.,  $n = 10$ , RP 22.4 years, Figure 7).

## 4 | Discussion

Co-occurring flooding and extreme wind in GB are part of a complex multi-hazard risk to society (e.g., Simpson et al. 2021),

and this paper considers these hazards using impact-based proxies (Hillier and Dixon 2020), the UKCP18r dataset and modelled river flows (Griffin, Kay, Sayers, et al. 2024). Its aim is to understand the joint hazard and its drivers. Other complexities, such as interactions between vulnerabilities or exposed infrastructure systems, are not considered. This paper offers:

1. A first examination of the jet stream for events based on high-flow conditions, not extreme rainfall, in a sentinel location for NW Europe
2. A multi-temporal ( $\Delta t = 1$ – $180$  days) approach that groups events into multi-hazard *episodes* in a way that is relevant to stakeholders.
3. A new set of 3427 wind events.
4. An examination of the role of seasonality in how high flows and extreme wind co-occur.
5. An assessment of relatively simple jet stream metrics (Woollings, Hannachi, and Hoskins 2010) in this context.

The work fits into a growing consensus on various aspects of potential episodes of joint wintertime flooding and extreme wind in GB. These episodes are typically driven by extra-tropical cyclones (e.g., Hillier et al. 2015; Manning et al. 2024; Owen, Catto, Stephenson, et al. 2021; PERILS 2024), and associated with cyclonic or north-westerly weather patterns in an NAO+ regime (Bloomfield et al. 2024; Hillier et al. 2020). Figure 5 reinforces an doubling in frequency in future climate projections,

and also a x2-4 uplift ( $U$ ) in co-occurrence over a baseline of independence, a dependency that is not discernibly greater in future (Bloomfield et al. 2023; Manning et al. 2024). The jet stream associated with high river flows is to the south of GB, while for wind extremes it is to the north (Figure 7a), consistent with ETCs being rainy on their northern flank and windy to the south (Manning et al. 2024). And, Figure 7c shows that potential flooding tends to shift southwards in future (Bloomfield et al. 2024). It is also entirely in line with evidence that GB in future will be wetter (e.g., Lane and Kay 2021; Lowe et al. 2019) with more frequent and severe high-flows (Collet et al. 2018; Griffin, Kay, Sayers, et al. 2024). Despite being heavily validated, a caveat is that these studies rely on UKCP18r using the RCP8.5 emissions scenario, highlighting the need for a multi-model study or other emission scenarios. An important aspect of the agreement across varied approaches is that it demonstrates, through the episode definition used here, that previous work is applicable to (re)insurance and other stakeholders and their experience of episodes.

On this theme, what is an appropriate baseline? Namely, what statistical model (e.g., days of non-severe storms, uniform occurrence in DJF) should be chosen to represent independence between hazards for a particular enquiry? An insurer's standard practice might involve independence across an October–March season today. Then, illustratively (at  $\Delta t=21$ )  $\varepsilon_F^{95}$  has a 1-year RP and  $\varepsilon_W^{95}$  has a 1-year RP, combining to be a 22-year RP joint episode assuming the  $R_{\text{day}}$  model, which is reduced fourfold to a 6-year RP in 2061–2079 accounting for dependence (Figure 6b,c). If an insurer's modelling correctly includes the individual hazards seasonality, the correction needed would be notably less (Figure 6). Thus, a fixed timeframe for analysis such as DJF or October–March (e.g., Zscheischler et al. 2021) should be used with caution, especially since peak months of (co-)occurrence may shift in future, and practitioners and researchers must ensure the statistical approach aligns with the research question posed.

Selected aspects of the results are now discussed.

#### 4.1 | Co-Occurrence for the Most Extreme Events

The initial estimate of uplift in co-occurrence between extreme winds and high-flow in rivers was ~1.5 times (Hillier et al. 2015). A value of ~2–4 times in UKCP18r for daily data (Bloomfield et al. 2023) is now confirmed visually (Figure 4) and statistically (Figures 5 and Figure 6) for episodes like to cause loss (Appendix A4), and appears robust in that it is not overly dependent on the method, metrics, or time period (1981–1999, or 2061–2079) used in the studies. Less well constrained is whether, in the limit, are these perils are asymptotically dependent or independent? Namely, do the most severe events have a weaker or stronger tendency to co-occur? This is a key question in assessing risk.

For ERA5 wind gusts and precipitation or GLOFAS derived river flow (at daily, weekly, monthly resolution), residual tail dependence ( $\bar{\chi}$ ) (Coles, Heffernan, and Tawn 1999) does not tend to 1.0 as required for asymptotic dependence, but equally gives no indication that correlation disappears into the tail of

the distribution, with the same true for monthly Network Rail delay data (Bloomfield et al. 2023; Vignotto, Engelke, and Zscheischler 2021). Indeed, in UKCP18r uplift  $U$  increases from 2.4 to 3.4 as Bloomfield's threshold increases, an effect previously demonstrated by sensitivity testing (Hillier and Dixon 2020). Figure 5 extends this, with systematic increases in  $U$  from the 75th to 99th percentile ( $\varepsilon_J^{75}$  to  $\varepsilon_J^{99}$ ) indicating that more extreme episodes co-occur more strongly (Figure 5a,b), at least to return periods of up to ~50–100 years (Figure 5c,d).

Other metrics give a different view. Even as  $\bar{\chi}$  or  $U$  increase or hold steady with increasing threshold,  $\chi$  and Spearman's  $r$  decrease (Bloomfield et al. 2023; Hillier and Dixon 2020). Taking this further, for rain and wind, with a Clayton copula best fitting their severity metrics for (UKCP18, 2.2 km) Manning et al. (2024) implicitly assume asymptotic independence for the most extreme events. Indeed, by taking parts of two winter seasons and summer (i.e., January–December) it is possible to find negative correlations at higher thresholds and annual timeframes (Jones, Stephenson, and Priestley 2024). The variety highlights the importance of using measures attuned to each study's purpose.  $U$  is a statistic that directly comments on the chance of two extreme events in a season, as in some stress tests for insurers (Bank of England 2022). It could also be used to force dependency between independently derived (i.e., uncorrelated) event sets at selected percentile(s) (e.g., 75th, 95th, 99th) perhaps with copulas (e.g., Hillier et al. 2023) to better estimate actual likely losses, improving on using one Spearman's  $r$  value to represent dependency for all events causing notable losses (Hillier et al. 2024). Given these apparent discrepancies, it would be beneficial to further investigate extreme winds and high river flows or flooding, perhaps with larger model ensembles.

#### 4.2 | Co-Occurrence Across Timeframes

How does strength of co-occurrence vary with the time-window ( $\Delta t$ ) used to group events? Previous wind-flow work using Spearman's  $r$  on regular, non-overlapping periods found it to increase for windows of up to 20–40 days and then hold steady, perhaps decreasing slightly for a whole season (Bloomfield et al. 2023). Figure 5, however, uses a measure of tail dependency to focus on the severe events ( $\varepsilon_J^{75}$ ) thought to best represent impactful events (Bloomfield et al. 2023, Appendix A4), and indicates that uplift ( $U$ ) is highest for shorter time windows. Assuming UKCP18 correctly captures persistence, this overturns the working hypothesis in the initial papers (Hillier et al. 2015; Hillier and Dixon 2020). These looked at seasonal timescales, as the prevailing yet unpublished view in 2015 was that individual storms were either wet or windy, and took evidence of wet and stormy winters (Kendon and McCarthy 2015; Matthews et al. 2014) to indicate that co-occurrence might most strongly exhibit on long timescales ( $\Delta t=180$ ). Descriptively and numerically, understanding this trend in strength of dependence with timeframe is useful for stakeholders who might have varied elements of their business to risk assess, from operational (e.g., 3 day or 21 day long event durations in insurance contracts, or railway repairs) to planning (e.g., annual regulatory or budgetary).

Understanding the relative dominance and interplay of the various hydrometeorological processes is less readily

achieved. The conceptual, multi-temporal model set out by Bloomfield et al. (2023) details evidence for shorter-term ( $\Delta t \approx 1\text{--}15$  days) contributions from storms (i.e., sub-storm to storm clusters) and longer term ‘memory’, perhaps in GB groundwater or distant conditions (De Luca et al. 2017; Hillier et al. 2015) mediated by atmospheric behaviours captured by weather patterns or the NAO index (Bloomfield et al. 2024; e.g., Hillier et al. 2020). While winters in GB and NW Europe can be undoubtably wet and stormy (Met Office 2024), the pattern in Figure 5 adds weight to a case that processes at shorter timescales of a few weeks or less might dominate (i.e., storms, or storm sequences) rather than a set of conditions established for a season (e.g., Arctic sea-ice) dominating. But, any definite statement still seems premature. To aid progression to a process-orientated view, future statistical simulation modeling to split out contributions at the various time-scales (e.g., Hillier and Dixon 2020) with a consistent metric (e.g.,  $\chi$ ,  $U$ ,  $r$ ) is needed for high-flows and extreme wind. Meanwhile, a more in-depth look at the jet stream states associated with extreme winds and high flows can also contribute.

#### 4.3 | Utility of Simple Jet Stream Metrics

Extra-tropical cyclone (ETC) development is closely intertwined with the jet stream (Clark and Gray 2018; Dacre and Pinto 2020; e.g., Geng and Sugi 2001; Laurila et al. 2021). Illustratively, windstorms are located on its poleward side and are more intense when the jet is stronger (Laurila et al. 2021), and ETC clustering is more intense in GB with a strong persistent jet at  $\sim 50^\circ\text{N}$  (Pinto et al. 2014; Priestley et al. 2017). So, it was logical for Hillier and Dixon (2020) to propose the jet steam had a role in whether flooding and extreme wind co-occur or not based on an ETCs relationship with the jet.

Practically, calculating an index to quantify the jet stream (Ayles and Screen 2019; e.g., Woollings, Hannachi, and Hoskins 2010; Zappa, Pithan, and Shepherd 2018) is less demanding than cyclone tracking (e.g., Hoskins and Hodges 2002; Manning et al. 2024). So it is useful to ask if the relatively simply derived metrics for the eddy-driven (lower tropospheric) North Atlantic of jet of Woollings, Hannachi, and Hoskins 2010 can be a functional, readily applied tool to distinguish co-occurrence. If so, by being computationally easier than running cyclone tracking algorithms, it should facilitate inter-comparison of this potential driver of co-occurring high-flows and extreme wind between climate models and reanalyses (e.g., CMIP6, ERA5, UKCP).

Figure 7a,b,d,e clearly shows that the jet steam index of Woollings, Hannachi, and Hoskins 2010 is able to distinguish different large-scale jet dynamics associated with joint high-flow and wind events ( $\epsilon_J^{75}$ , dark red line), providing an easy answer to the question posed about utility. Specifically, wind ( $\epsilon_W^{95}$ ) and  $\epsilon_J^{75}$  episodes have a stronger jet than high-flows ( $\epsilon_F^{95}$ ), in accord with analysis of extreme precipitation and expectations that a weaker jet causes ETCs to move more slowly allowing rainfall to persist for longer (Hillier and Dixon 2020; Manning et al. 2024). Indeed, Figure 7 demonstrates how statistical significance testing using jet metrics can support this idea, augmenting visual analysis (Manning et al. 2024). In future (2061–2079) latitude illustrates a case where signatures of

subsets are similar, with distinctions not clear-cut using only this index (Figure 7c). So other views, such as on the timing of episodes within a season or their planform distributions of associated high-level wind (Figures 6 and 8), are also useful to understand the influence of the jet stream.

#### 4.4 | Potential Influences of the Jet Stream on Future Co-Occurrence

Do dynamical (e.g., jet stream) or thermodynamic effects most control the co-occurrence? Previous analysis has inferred that the future increase in co-occurrence is a predominantly thermodynamic response (i.e., warmer air can be wetter, and therefore more high FSI events), assisted by southwards displaced cyclone tracks leading to dynamically enhanced temperature (Manning et al. 2024). Figures 6–8 allows this to be clarified.

First, consider 21 day episodes (Figure 6a–c), likely associated with storm sequences (e.g., Bloomfield et al. 2023; Dacre and Pinto 2020; Mühr et al. 2022). For a start, simply doubling the number of high-flow events during October–March in a wetter future world is insufficient ( $R_{\text{day}}$ , Figure 6c). Interestingly, both high-flows and wind extremes become more seasonal, focused into midwinter, particularly with higher percentiles (Figure 6a,d, Appendices A and B). An increased frequency of high flows across winter as a whole is an established idea (Griffin, Kay, Sayers, et al. 2024), but within this the increased seasonality has not been noticed as the only relevant study lacked data over NW Europe (Ridder et al. 2020). Logically this phenomenon forces future co-occurrences to be more focussed in January (Figure 6c,f), and when this more intense seasonality is isolated and modelled ( $R_{\text{year}}$ ) it is nearly possible to explain the UKCP18r events (dark red line). So, at this time-frame, if atmospheric drivers distribute extreme conditions correctly by month, thermodynamics are nearly sufficient to explain the increase in co-occurrence in future. Figure 7b,c demonstrates that mean UKCP18r jet stream latitude becomes more seasonal in future, in wintertime shifting south (equatorwards) and focussing on  $45^\circ\text{N}$  to impact GB. A stronger and squeezed future jet is in line with CMIP simulations (Oudar, Cattiaux, and Douville 2020; Peings et al. 2018), so a latitudinally squeezed wintertime jet might be the key dynamical driver of the increasingly seasonal future uptick in joint events. A equatorwards shift is in line with the Polar Amplification Model Intercomparison Project (PAMIP) findings where a sea-ice loss effect outweighs the polewards shift in the jet due to oceanic warming in this ‘tug-of-war’ (Screen et al. 2022). A northwards historical (1979–2019) shift of the jet stream has been reported in reanalysis products and climate model runs including UKCP18, inferred from a difference between mean zonal wind velocity (500 hPa) at  $40\text{--}50^\circ\text{N}$  as compared to  $20\text{--}30^\circ\text{N}$  (Woollings et al. 2023). This, however, is readily reconciled with our finding of a potential future southerly shift in the jet and that of ETC tracks (Manning et al. 2024), by considering Figure 6b,c. In DJF, in the Atlantic at least, there is a southwards shift of the jet into the  $40\text{--}50^\circ\text{N}$  bin, increasing typical wind speeds there with respect to that at  $20\text{--}30^\circ\text{N}$ . So, Figure 6 provides an additional insight into how broad-scale thermodynamic and dynamic factors combine to explain longer joint high-flow and wind episodes.

For individual or closely consecutive storms ( $\Delta t = 3$  days), Figure 6e,f clearly shows that the number of events alone is insufficient to cause the co-occurrences in UKCP18r, particularly in the future, even if enhanced seasonality is accounted for (red line,  $R_{\text{year}}$ ). So, another shorter-term explanatory atmospheric behaviour is needed. Figures 7 and 8 suggest that this is the disposition and dynamics of the jet stream. In terms of the latitude and speed of the jet's strongest part, the typical mid-winter jet becomes more like that characteristic of impactful compound storms today (Figure 7). Figure 8 adds plan-view information on the jet at the time of high joint FSI-SSI episodes impact GB. In the present, joint episodes ( $\epsilon_j^{75}$ ) have a jet that typically blends most of the strength of wind events ( $\epsilon_W^{95}$ ) with the more southerly track of high-flow inducing events ( $\epsilon_F^{95}$ ). In future, a stronger and more southerly jet is much more prominent for  $\epsilon_j^{75}$  episodes (Figures 7c and 8e), fitting with the location of extreme precipitation (Bloomfield et al. 2024) and its associated jet (Manning et al. 2024) moving south.

Future high FSI-SSI episodes ( $\epsilon_j^{75}$ ) better resemble wind episodes than high-flow (Figure 8d-f), fitting with a view of a typically rainy wintertime future GB where wind is typically the missing element for a joint event (Bloomfield et al. 2024). Namely, wind becomes the limiting factor rather than flooding as it is now; currently multi-basin high-flows needs multiple storms setting wet antecedent conditions (De Luca et al. 2017), and locally the joint impact footprint's extent is limited by its rain component (Manning et al. 2024). Intriguingly, a southerly jet anomaly during a compound storm's lifetime over the Atlantic (Figure A1—Manning et al. 2024) that obtains a very windy signature when impacting GB (Figure 8d,f) suggests the most severe future events might arise from a jet initially passing over warm southerly water that strengthens and shifts north as it impacts southern GB. So, in a modification to the conclusion of Manning et al. (2024) a relatively equal contribution of dynamics (i.e., jet disposition and seasonality) and thermodynamical (i.e., warmer air carries more moisture) is argued to drive future increases in joint hazard in GB.

Placing an emphasis on dynamics (e.g., jet stream) ties in with a broader, emerging picture of linked multi-hazards across the Atlantic domain (e.g., Röhlisberger, Pfahl, and Martius 2016). Cold air outbreaks over eastern Canada followed by wind extremes over northern Europe and the British Isles appear associated with an enhanced jet stream (Leeding, Riboldi, and Messori 2023), while January being the dominant month for compound surge and rainfall around GB (Bevacqua et al. 2020) ties to the same timing for wind and riverine high-flows (Figure 6). Furthermore, clustered ETC are associated with a jet stream anomaly focussed on GB (Dacre and Pinto 2020; Pinto et al. 2014; Priestley et al. 2017). And, like flow regimes globally, these relationships are likely to change with the climate (e.g., Jiménez Cisnero and Oki 2014; Li et al. 2024). We therefore advocate a process-orientated approach to co-occurring hazards (e.g., Manning et al. 2024), highlight that the 'recipe' of driving large-scale conditions (e.g., jet stream state) for such a 'perfect storm' (e.g., Hillier et al. 2023) will vary by country (Gonçalves, Nieto, and Liberato 2023; Raveh-Rubin 2015; Röhlisberger, Pfahl, and Martius 2016), and advocate the application of our novel methods in other regions.

## 5 | Conclusions

This study uses novel statistical modelling of dependencies and a jet stream index (Woollings, Hannachi, and Hoskins 2010) to understand the co-occurrence of high-flows and extreme wind events in multi-hazard *episodes*, with a focus on 3-day and 21-day durations. The idea of dynamically defined episodes that group events to reflect periods of adverse conditions is defined to reflect lived experience, and extracted using the FSI (Bloomfield et al. 2023, 2024) and SSI indices (e.g., Klawa and Ulbrich 2003) from the UKCP18 regional 12 km dataset which has previously been validated (Bloomfield et al. 2023). The main conclusions are:

- Defining stormy multi-event episodes as they are experienced (i.e., dynamically positioned time windows) produces results that align with previous work, giving stakeholders additional comfort in using published results.
- This said, statistically, it is critical to note that different dependency measures (e.g.,  $\chi$ ,  $U$ ,  $r$ ,  $\tau$ ) reflect different aspects of distributions of joint extremes, and may even appear contradictory. Also, using fixed timeframe for analysis (e.g., October–March, DJF) should be used with caution, especially since peak months may shift in future. Statistically modelling seasonality in a month-by-month analysis as done here may be necessary.
- Uplift ( $U$ ) in co-occurrence is found to increase as severity increases (e.g., 90th to 99th percentile), meaning that evidence is starting to suggest that dependence exists to high return periods, even if not strictly 'asymptotic'. So, ignoring correlation underestimates risk most for the strongest storms.
- Uplift is found to increase as  $\Delta t$  is reduced, highest within insurers' key windows ( $\Delta t = 3$  and 21 days), suggesting the importance of atmospheric mechanisms that act to drive co-occurrence at timescales of days to weeks (e.g., storm sequences); see the framework model in Bloomfield et al. (2023). So, ignoring correlation underestimates risk most for individual or closely grouped storms.
- Jet stream metrics (e.g., Woollings, Hannachi, and Hoskins 2010) are found to be a useful, easily determined tool to investigate its roles as a driver of co-occurrence.
- Future strong jet streams become increasingly focussed in mid-winter (December–February) driving the increased seasonality in individual hazards, a larger effect for more extreme events. This broad-scale dynamic effect, combined with thermodynamics (i.e., a warmer, wetter world), explains most of the uplift in future joint events at storm-sequence timescales ( $\Delta t = 21$  days) and over.
- For individual or closely consecutive storms ( $\Delta t = 3$  days), altered jet characteristics are also needed to fully explain the uplift in co-occurrence, stronger and displaced southwards as storms impact GB. In short, typical future DJF jet variability closely resembles that of impactful compound storms in GB today highlighting the contribution of the jet changes to the increase in extremes.

Future work will could unpick and quantify the balance between dynamic and thermodynamic effects, ideally using higher

resolution data from a variety of climate models. It will be important, however, to build area-by-area understanding of how the impact of common drivers varies spatially to improve risk mitigation and planning (e.g., diversification, mutual aid across Europe). As the jet stream guides storms to one region, another will be spared.

## Author Contributions

**John K. Hillier:** writing – original draft, funding acquisition, investigation, conceptualization, methodology, visualization, writing – review and editing, formal analysis. **Hannah C. Bloomfield:** writing – review and editing, conceptualization, formal analysis, investigation. **Colin Manning:** writing – review and editing. **Freya Garry:** writing – review and editing. **Len Shaffrey:** conceptualization, writing – review and editing. **Paul Bates:** writing – review and editing, conceptualization. **Dhirendra Kumar:** visualization.

## Acknowledgements

To undertake this work Hillier was funded by a NERC, UK Knowledge Exchange Fellowship (Grant Number NE/V018698/1). Bloomfield, Shaffrey, Bates and Kumar are part-supported by the UK Centre for Greening Finance and Investment (NERC CGFI Grant Number NE/V017756/1), which Hillier is associated with as an Associate Research Fellow. Thanks are given to Adam Griffin at CEH and the AquaCAT project, who developed the UKCP18r based river flow simulations, advised about them and provided a daily time-series to accompany them. Garry and the AquaCAT project were funded under the UK Research and Innovation Strategic Priorities Fund UK Climate Resilience programme, co-delivered by Met Office and NERC on behalf of UKRI partners AHRC, EPSRC and ESRC.

## Conflicts of Interest

The authors declare no conflicts of interest.

## Data Availability Statement

UKCP18 data are available from the Met Office. Flooding events are from Griffin, Kay, Bell, et al. (2022) on the CEDA repository. Wind and precipitation events are available on Zenodo (doi: 10.5281/zenodo.14282051, <https://zenodo.org/records/14282051>) and have been submitted to the CEDA archive (<https://archive.ceda.ac.uk/>).

## References

Ayres, H. C., and J. A. Screen. 2019. "Multimodel Analysis of the Atmospheric Response to Antarctic Sea Ice Loss at Quadrupled CO<sub>2</sub>." *Geophysical Research Letters* 46: 9861–9869. <https://doi.org/10.1029/2019GL083653>.

Bank of England. 2022. "General Insurance Stress Test 2022—Scenario Specification, Guidelines and Instructions".

Berghuijs, W. R., S. Harrigan, P. Molnar, L. Slater, and J. W. Kirchner. 2019. "The Relative Importance of Different Flood-Generating Mechanisms Across Europe." *Water Resources Research* 55: 4582–4593. <https://doi.org/10.1029/2019WR024841>.

Bevacqua, E., C. De Michele, C. Manning, et al. 2021. "Guidelines for Studying Diverse Types of Compound Weather and Climate Events." *Earth's Future* 9: e2021EF002340. <https://doi.org/10.1029/2021EF002340>.

Bevacqua, E., D. Maraun, H. I. Haff, M. Widmann, and M. Vrac. 2017. "Multivariate Statistical Modelling of Compound Events via Pair-Copula Constructions: Analysis of Floods in Ravenna (Italy)." *Hydrology and Earth System Sciences* 21: 2701–2723.

Bevacqua, E., V. I. Voudoukas, G. Zappa, et al. 2020. "More Meteorological Events That Drive Compound Coastal Flooding Are Projected Under Climate Change." *Communications Earth & Environment* 1: 47. <https://doi.org/10.1038/s43247-020-00044-z>.

Bister, M., and K. Emanuel. 1998. "Dissipative Heating and Hurricane Intensity." *Meteorology and Atmospheric Physics* 65: 233–240.

Black, A. R., and F. M. Law. 2004. "Development and Utilization of a National Web-Based Chronology of Hydrological Events/ Développement et Utilisation sur Internet d'une Chronologie Nationale d'événements Hydrologiques." *Hydrological Sciences Journal* 49: 237–246. <https://doi.org/10.1623/hysj.49.2.237.34835>.

Bloomfield, H., J. K. Hillier, A. Griffin, et al. 2023. "Co-Occurring Wintertime Flooding and Extreme Wind Over Europe, From Daily to Seasonal Timescales." *Weather and Climate Extremes* 39: 100550. <https://doi.org/10.1016/j.wace.2023.100550>.

Bloomfield, H. C., P. D. Bates, L. C. Schaffrey, et al. 2024. "Synoptic Conditions Conducive for Compound Wind-Flood Events in Great Britain in Present and Future Climates." *Environmental Research Letters* 19: 024019. <https://doi.org/10.1088/1748-9326/ad1cb7>.

Böllman, G., and G. Jurksch. 1984. "Ein Beitrag zur Festlegung der Grundwind- und Nennböengeschwindigkeit im Binnenland der Bundesrepublik Deutschland für die DIN-NORM 1055, Teil 4." *Meteor Rdsch* 37: 1–10.

Businger, S., and J. Businger. 2001. "Viscous Dissipation of Turbulence Kinetic Energy in Storms." *Journal of the Atmospheric Sciences* 58: 3793–3796.

CCC. 2022. Winter Windstorm Indicators for Europe From 1979 to 2021 Derived From Reanalysis. <https://doi.org/10.24381/cds.9b4ea013>. Copernicus Climate Change Service (C3S), Climate Data Store (CDS).

Champion, A. J., R. P. Allan, and D. A. Lavers. 2015. "Atmospheric Rivers Do Not Explain UK Summer Extreme Rainfall." *Journal of Geophysical Research: Atmospheres* 120: 6731–6741. <https://doi.org/10.1002/2014JD022863>.

Chandler, A. M., E. J. W. Jones, and M. H. Patel. 2001. "Property Loss Estimation for Wind and Earthquake Perils." *Risk Analysis* 21: 235–249. <https://doi.org/10.1111/0272-4332.212108>.

Christofides, S., C. Barlow, N. Michaelides, and C. Miranthis. 1992. *Storm Rating in the Nineties*, 5–89. London, UK: General Insurance Convention.

Claassen, J., P. J. Ward, J. E. Daniell, E. E. Koks, T. Tiggeloven, and M. C. de Ruiter. 2023. "A New Method to Compile Global Multi-Hazard Event Sets." *Scientific Reports* 13: 13808. <https://doi.org/10.1038/s41598-023-40400-5>.

Clark, P. A., and S. L. Gray. 2018. "Sting Jets in Extratropical Cyclones: A Review." *Quarterly Journal of the Royal Meteorological Society* 148: 943–969. <https://doi.org/10.1002/qj.3267>.

Coles, S., J. Heffernan, and J. Tawn. 1999. "Dependence Measures for Extreme Value Analyses." *Extremes* 2: 339–365. <https://doi.org/10.1023/A:1009963131610>.

Collet, L., S. Harrigan, C. Prudhomme, G. Formetta, and L. Beavers. 2018. "Future Hot-Spots for Hydro-Hazards in Great Britain: A Probabilistic Assessment." *Hydrology and Earth System Sciences* 22: 5387–5401. <https://doi.org/10.5194/hess-22-5387-2018>.

Cotterill, D., P. Stott, N. Christidis, and E. Kendon. 2021. "Increase in the Frequency of Extreme Daily Precipitation in the United Kingdom in Autumn." *Weather and Climate Extremes* 33: 100340. <https://doi.org/10.1016/j.wace.2021.100340>.

Dacre, H. F., and J. G. Pinto. 2020. "Serial Clustering of Extratropical Cyclones: A Review of Where, When and Why It Occurs, Npj Climate and Atmospheric." *Science* 3: 1–10. <https://doi.org/10.1038/s41612-020-00152-9>.

De Luca, P., J. K. Hillier, R. L. Wilby, N. W. Quinn, and S. Harrigan. 2017. "Extreme Multi-Basin Flooding Linked With Extra-Tropical Cyclones." *Environmental Research Letters* 12: 114009. <https://doi.org/10.3390/atmos10100577>.

de Ruiter, M., A. Couasnon, M. J. C. van den Homberg, J. E. Daniell, J. Gill, and P. J. Ward. 2019. "Why We Can No Longer Ignore Consecutive Disasters, Earth's." *Futures* 8: e2019EF001425. <https://doi.org/10.1029/2019EF001425>.

Dixon, R., C. Souch, and D. Whitaker. 2017. *European Windstorm: Needs of the Insurance Industry*, 21–23. Reading, UK: Lighthill Risk Network. <http://www.stormworkshops.org/workshop2017.html>.

Donges, J. F., C. F. Schleussner, J. F. Siegmund, and R. V. Donner. 2016. "Event Coincidence Analysis for Quantifying Statistical Interrelationships Between Event Time Series." *European Physical Journal Special Topics* 225: 471–487. <https://doi.org/10.1140/epjst/e2015-50233-y>.

Dorland, C., R. S. J. Tol, and J. Palutikof. 1999. "Vulnerability of the Netherlands and Northwest Europe to Storm Damage Under Climate Change." *Climate Change* 43: 513–535.

Emanuel, K. 1998. "The Power of a Hurricane: An Example of Reckless Driving on the Information Superhighway." *Weather* 54: 107–108.

Emanuel, K. 2005. "Increasing Destructiveness of Tropical Cyclones Over the Past 30 Years." *Nature* 436: 686–688.

Escobar, M. 2015. "Studying Coincidences With Network Analysis and Other Multivariate Tools." *Stata Journal* 15: 1118–1156.

European Environment Agency. 2024. Economic Losses From Weather- and Climate-Related Extremes in Europe.

Fink, A. H., T. Brucher, V. Ermert, A. Kruger, and J. G. Pinto. 2009. "The European Storm Kyrill in January 2007: Synoptic Evolution, Meteorological Impacts and Some Considerations With Respect to Climate Change." *Natural Hazards and Earth System Sciences* 9: 405–423.

Gallina, V., S. Torresan, A. Critto, A. Sperotto, T. Glade, and A. Marcomini. 2016. "A Review of Multi-Risk Methodologies for Natural Hazards: Consequences and Challenges for a Climate Change Impact Assessment." *Journal of Environmental Management* 168: 123–132. <https://doi.org/10.1016/j.jenvman.2015.11.011>.

Geng, Q., and M. Sugi. 2001. "Variability of the North Atlantic Cyclone Activity in Winter Analyzed From NCEP–NCAR Reanalysis Data." *Journal of Climate* 14: 3863–3873.

Gonçalves, A. C. R., R. Nieto, and M. L. R. Liberato. 2023. "Synoptic and Dynamical Characteristics of High-Impact Storms Affecting the Iberian Peninsula During the 2018–2021 Extended Winters." *Atmosphere* 14: 1353. <https://doi.org/10.3390/atmos14091353>.

Griffin, A., A. Kay, V. Bell, E. Stewart, P. Sayers, and S. Carr. 2022. "Peak Flow and Probability of Exceedance Data for Grid-To-Grid Modelled Widespread Flooding Events Across Mainland GB From 1980–2010 and 2050–2080." <https://doi.org/10.5285/26ce15dd-f994-40e0-8a09-5f257cc1f2ab>.

Griffin, A., A. L. Kay, P. Sayers, E. Bell, and S. Carr. 2024. "Widespread Flooding Dynamics Changing Under Climate Change: Characterising Floods Using Grid-Based Hydrological Modelling and Regional Climate Projections." *Hydrology and Earth System Sciences Discussions* 28, no. 12: 1–18. <https://doi.org/10.5194/hess-2022-243>.

Hadzilicos, G., R. Li, P. Harrington, et al. 2021. *It's Windy When it's Wet: Why UK Insurers May Need to Reassess Their Modelling Assumptions*. London, UK: Bank Underground.

Harrigan, S., E. Zoster, H. Cloke, P. Salamon, and C. Prudhomme. 2023. "Daily Ensemble River Discharge Reforecasts and Real-Time Forecasts From the Operational Global Flood Awareness System." *Hydrology and Earth System Sciences* 27: 1–19. <https://doi.org/10.5194/hess-27-1-2023>.

Heffernan, J., and J. Tawn. 2004. "A Conditional Approach for Multivariate Extreme Values." *Journal of the Royal Statistical Society, Series B* 66: 169–182.

Heneka, P., T. Hofherr, B. Ruck, and C. Kottmeier. 2006. "Winter Storm Risk of Residential Structures—Model Development and Application to the German State of Baden-Württemberg." *Natural Hazards and Earth System Sciences* 6: 721–733. <https://doi.org/10.5194/nhess-6-721-2006>.

Heneka, P., and B. Ruck. 2008. "A Damage Model for the Assessment of Storm Damage to Buildings." *Engineering Structures* 30: 3603–3609. <https://doi.org/10.1016/j.engstruct.2008.06.005>.

Hersbach, H., B. Bell, P. Berrisford, et al. 2020. "The ERA5 Global Reanalysis." *Quarterly Journal of the Royal Meteorological Society* 146: 1999–2049. <https://doi.org/10.1002/qj.3803>.

Hewitt, K., and I. Burton. 1971. *Hazardousness of a Place: A Regional Ecology of Damaging Events*, 154. Toronto, Canada: Toronto Press.

Hewston, R., and S. R. Dorling. 2011. "An Analysis of Observed Daily Maximum Wind Gusts in the UK." *Journal of Wind Engineering and Industrial Aerodynamics* 99: 845–856. <https://doi.org/10.1016/j.jweia.2011.06.004>.

Hill, M., D. Gately, and N. Peiris. 2013. "Damage Observations in the UK From Windstorm Ulli and Implications for Building Codes and Loss Estimation." In *6th European and African Conference on Wind Engineering, 7th–14th July 2013, Cambridge, UK*, 1–8.

Hillier, J. K. 2017. "The Perils in Brief." In *Natural Catastrophe Risk Management and Modelling: A Practitioner's Guide*, vol. 536. Oxford, UK: Wiley-Blackwell.

Hillier, J. K., A. Champion, T. Perkins, F. Garry, and H. Bloomfield. 2024. "GC Insights: Open R-Code to Communicate the Impact of Co-Occurring Natural Hazards." *Geoscience Communication Discussions* 7: 195–200. <https://doi.org/10.5194/egusphere-2023-2799>.

Hillier, J. K., and R. Dixon. 2020. "Seasonal Impact-Based Mapping of Compound Hazards." *Environmental Research Letters* 15: 114013. <https://doi.org/10.1088/1748-9326/abbc3d>.

Hillier, J. K., N. Macdonald, G. C. Leckebusch, and A. Stavrinides. 2015. "Interactions Between Apparently Primary Weather-Driven Hazards and Their Cost." *Environmental Research Letters* 10: 104003. <https://doi.org/10.1088/1748-9326/10/10/104003>.

Hillier, J. K., T. Matthews, R. L. Wilby, and C. Murphy. 2020. "Multi-Hazard Dependencies Can Increase and Decrease Risk." *Nature Climate Change* 10: 595–598. <https://doi.org/10.1038/s41558-020-0832-y>.

Hillier, J. K., T. Perkins, R. Li, et al. 2023. *What if it's a Perfect Storm? Bank Underground: Stronger Evidence That Insurers Should Account For Co-Occurring Weather Hazards*.

Hillier, J. K., and M. Van Meeteren. 2024. "Co-RISK: A Tool to Co-Create Impactful University-Industry Projects for Natural Hazard Risk Mitigation." *Geoscience Communication* 7: 35–56. <https://doi.org/10.5194/gc-7-35-2024>.

Hirpa, F. A., P. Salamon, H. E. Beck, et al. 2018. "Calibration of the Global Flood Awareness System (GloFAS) Using Daily Streamflow Data." *Journal of Hydrology* 566: 595–606.

Hoskins, B., and K. Hodges. 2002. "New Perspectives on the Northern Hemisphere Winter Storm Tracks." *Journal of Atmospheric Sciences* 59: 1041–1061.

Jacob, D., J. Petersen, B. Eggert, et al. 2014. "EURO-CORDEX: New High-Resolution Climate Change Projections for European Impact Research." *Regional Environmental Change* 14: 563–578. <https://doi.org/10.1007/s10113-013-0499-2>.

Jiménez Cisnero, B. E., and T. Oki. 2014. "Part A: Global and Sectoral Aspects." In *Contribution of Working Group II to the Fifth Assessment Report of the Intergovernmental Panel on Climate Change*, in: *Climate*

*Change 2014: Impacts, Adaptation, and Vulnerability*, 229–269. Cambridge, UK: Cambridge University Press.

Jones, T., D. B. Stephenson, and M. K. Priestley. 2024. “Correlation of Wind and Precipitation Annual Aggregate Severity of European Cyclones.” *Weather* 79: 176–181. <https://doi.org/10.1002/wea.4573>.

Kappes, M. S., M. Keiler, K. von Elverfeldt, and T. Glade. 2012. “Challenges of Analyzing Mult-Hazard Risk: A Review.” *Natural Hazards* 64: 1925–1958. <https://doi.org/10.1007/s11069-012-0294-2>.

Kay, A., A. Griffin, A. Rudd, R. Chapman, V. Bell, and N. Arnell. 2021. “Climate Change Effects on Indicators of High and Low River Flow Across Great Britain.” *Advances in Water Resources* 151: 103909. <https://doi.org/10.1016/j.advwatres.2021.103909>.

Kendon, M. 2022. “Storms Dudley, Eunice and Franklin February 2022.” Technical Report. Met Office.

Kendon, M., and M. McCarthy. 2015. “The UK’s Wet and Stormy Winter of 2013/2014.” *Weather* 7: 40–47.

Klawa, M., and U. Ulbrich. 2003. “A Model for the Estimation of Storm Losses and the Identification of Severe Winter Storms in Germany.” *Natural Hazards and Earth System Sciences* 3: 725–732.

Kopp, J., P. Rivoire, S. M. Ali, Y. Barton, and O. Martius. 2021. “A Novel Method to Identify Sub-Seasonal Clustering Episodes of Extreme Precipitation Events and Their Contributions to Large Accumulation Periods.” *Hydrology and Earth System Sciences* 25: 5153–5174. <https://doi.org/10.5194/hess-25-5153-2021>.

Küpfer, K. 2024. “Impact-Based Event Catalogue on Serially Clustered Extreme Events of Different Types in South-West Germany.” *EGU Sphere*. <https://doi.org/10.5194/egusphere-2024-2803>.

Lane, R. A., and A. Kay. 2021. “L.: Climate Change Impact on the Magnitude and Timing of Hydrological Extremes Across Great Britain.” *Frontiers in Water* 71: 684982. <https://doi.org/10.3389/frwa.2021.684982>.

Laurila, T. K., H. Gregow, J. Cornér, and V. A. Sinclair. 2021. “Characteristics of Extratropical Cyclones and Precursors to Windstorms in Northern Europe.” *Weather and Climate Dynamics* 2: 1111–1130. <https://doi.org/10.5194/wcd-2-1111-2021>.

Lechner, J. A., E. Simiu, and N. A. Heckert. 1993. “Assessment of ‘Peaks Over Threshold’ Methods for Estimating Extreme Value Distribution Tails.” *Structural Safety* 12: 305–314. [https://doi.org/10.1016/0167-4730\(93\)90059-A](https://doi.org/10.1016/0167-4730(93)90059-A).

Leckebusch, G. C., D. Renggli, and U. Ulbrich. 2008. “Development and Application of an Objective Storm Severity Measure for the Northeast Atlantic Region.” *Meteorologische Zeitschrift* 17: 575–587. <https://doi.org/10.1127/0941-2948/2008/0323>.

Leeding, R., J. Riboldi, and G. Messori. 2023. “On Pan-Atlantic Cold, Wet and Windy Compound Extremes.” *Weather and Climate Extremes* 39: 100524. <https://doi.org/10.1016/j.wace.2022.100524>.

Li, D., J. Zscheischler, Y. Chen, et al. 2024. “Intensification and Poleward Shift of Compound Wind and Precipitation Extremes in a Warmer Climate.” *Geophysical Research Letters* 51: e2024GL110135. <https://doi.org/10.1029/2024GL110135>.

Liberato, M. L. R. 2014. “The 19 January 2013 Windstorm Over the North Atlantic: Large-Scale Dynamics and Impacts on Iberia.” *Weather and Climate Extremes* 5–6: 16–28. <https://doi.org/10.1016/j.wace.2014.06.002>.

Lockwood, J., G. S. Guentchev, A. Alabaster, et al. 2022. “Using High-Resolution Global Climate Models From the PRIMAVERA Project to Create a European Winter Windstorm Event Set.” *Natural Hazards and Earth System Sciences* 22: 3585–3606. <https://doi.org/10.5194/nhess-22-3585-2022>.

Lowe, J. A., D. Bernie, P. Bett, et al. 2019. *UKCP18 Science Overview Report*. Exeter, UK: Met Office.

Mailier, P. J., D. B. Stephenson, C. A. T. Ferro, and K. I. Hodges. 2006. “Serial Clustering of Extratropical Cyclones.” *Monthly Weather Review* 134: 2224–2240. <https://doi.org/10.1175/MWR3160.1>.

Manning, C., E. J. Kendon, H. J. Fowler, J. L. Katto, S. C. Chan, and P. G. Sansom. 2024. “Compound Wind and Rainfall Extremes: Drivers and Future Changes Over the UK and Ireland.” *Weather and Climate Extremes* 44: 100673. <https://doi.org/10.1016/j.wace.2024.100673>.

Manning, C., E. J. Kendon, H. J. Fowler, and N. M. Roberts. 2023. “Projected Increase in Windstorm Severity and Contribution From Sting Jets Over the UK and Ireland.” *Weather and Climate Extremes* 40: 100562. <https://doi.org/10.1016/j.wace.2023.100562>.

Manning, C., E. J. Kendon, H. J. Fowler, et al. 2022. “Extreme Windstorms and Sting Jets in Convection-Permitting Climate Simulations Over Europe.” *Climate Dynamics* 58: 2387–2404. <https://doi.org/10.1007/s00382-021-06011-4>.

Manning, C., Kendon, E. J., Fowler, H. J., Katto, J. L., Chan, S. C., and Sansom, P. G. 2024. “Compound Wind and Rainfall Extremes: Drivers and Future Changes Over the UK and Ireland.” *Weather and Climate Extremes* 44: 100673. <https://doi.org/10.1016/j.wace.2024.100673>.

Martius, O., S. Pfahl, and C. Chevalier. 2016. “A Global Quantification of Compound Precipitation and Wind Extremes: Compound Precipitation and Wind Extremes.” *Geophysical Research Letters* 43: 7709–7714. <https://doi.org/10.1002/2016GL070017>.

Matthews, T., C. Murphy, G. McCarthy, C. Broderik, and R. L. Wilby. 2018. “Super Storm Desmond: A Process-Based Assessment.” *Environmental Research Letters* 13: 014024.

Matthews, T., C. Murphy, R. L. Wilby, and S. Harrigan. 2014. “Stormiest Winter on Record for Ireland and UK.” *Nature Climate Change* 4: 738–740. <https://doi.org/10.1038/nclimate2336>.

McSweeney, C., and P. Bett. 2020. *UKCP European Circulation Indices: Jet Stream Position and Strength*, UKCP Factsheet. Exeter, UK: Met Office, Hadley Centre.

Met Office. 2024. “UK Storm Centre, Warnings and Advice.”

Mitchell-Wallace, K., M. Jones, J. K. Hillier, and M. Foote. 2017. *Natural Catastrophe Risk Management and Modelling: A Practitioner’s Guide*, 506. Oxford, UK: Wiley.

Mühr, B., L. Eisenstein, G. J. Pinto, P. Knippertz, S. Mohr, and M. Kunz. 2022. *Winter Storm Series: Ylenia, Zeynep, Antonia (Int: Dudley, Eunice, Franklin) February 2022 (NW & Central Europe)*, Karlsruhe, Germany: KIT.

MunichRe. 2002. *Winter Storms in Europe (II): Analysis of 1999 Losses and Loss Potentials*. Munich, Germany: Munchener Rückversicherungs-Gesellschaft.

Murphy, J., G. Harris, D. Sexton, et al. 2018. *UKCP18 Land Projections: Science Report*. Met Office: Exeter.

Osinski, R., P. Lorenz, T. Kruschke, et al. 2016. “An Approach to Build an Event Set of European Wind Storms Based on ECMWF EPS.” *Natural Hazards and Earth System Sciences Discussions* 16: 255–268. <https://doi.org/10.5194/nhessd-3-1231-2015>.

Oudar, T., J. Cattiaux, and H. Douville. 2020. “Drivers of the Northern Extratropical Eddy-Driven Jet Change in CMIP5 and CMIP6 Models.” *Geophysical Research Letters* 47: e2019GL086695.

Owen, L. E., J. L. Catto, N. J. Dunstone, and D. S. Stephenson. 2021. “How Well Can a Seasonal Forecast System Represent Three Hourly Compound Wind and Precipitation Extremes Over Europe?” *Environmental Research Letters* 16: 074019. <https://doi.org/10.1088/1748-9326/ac092e>.

Owen, L. E., J. L. Catto, D. S. Stephenson, and N. J. Dunstone. 2021. “Compound Precipitation and Wind Extremes Over Europe and Their Relationship to Extratropical Cyclones.” *Weather and Climate Extremes* 33: 100342. <https://doi.org/10.1016/j.wace.2021.100342>.

Palutikof, J., and A. Skellern. 1991. *Storm Severity Over Britain, A Report to the Commercial Union General Insurance, Climatic Research Unit, School of Environmental Sciences*. Norwich, UK: Univeristy of East Anglia.

Pardowitz, T., R. Osinski, T. Kruschke, and U. Ulbrich. 2016. "An Analysis of Uncertainties and Skill in Forecasts of Winter Storm Losses." *Natural Hazards and Earth System Sciences* 16: 2391–2402. <https://doi.org/10.5194/nhess-16-2391-2016>.

Peings, Y., J. Cattiaux, S. J. Vavrus, and G. Magnusdottir. 2018. "Projected Squeezing of the Wintertime North-Atlantic Jet." *Environmental Research Letters* 074016. <https://doi.org/10.1088/1748-9326/aacc79>.

PERILS. 2023. "EUR 3,851M—PERILS Releases Final Industry Loss Estimate for February 2022." .European Windstorm Series.

PERILS. 2024. "Losses." Accessed 22 February 2024. <https://www.perils.org/losses>.

Pinto, J. G., I. Gómara, G. Masato, H. F. Dacre, T. Woolings, and R. Caballero. 2014. "Large-Scale Dynamics Associated With Clustering of Extratropical Cyclones Affecting Western Europe." *Journal of Geophysical Research* 119: 13–704. <https://doi.org/10.1002/2014JD022305>.

Pinto, J. G., M. K. Karremann, K. Born, P. M. Della-Marta, and M. Klawo. 2012. "Loss Potentials Associated With European Windstorms Under Future Climate Conditions." *Climate Research* 54: 1–20.

Prahl, B. F., D. Rybski, O. Burghoff, and J. P. Kropp. 2015. "Comparison of Storm Damage Functions and Their Performance." *Natural Hazards and Earth System Sciences* 15: 769–788. <https://doi.org/10.5149/nhess-15-769-2015>.

Prahl, B. F., D. Rybski, J. P. Kropp, and O. Burghoff. 2012. "Applying Stochastic Small-Scale Damage Functions to German Winter Storms." *Geophysical Research Letters* 39: L06806. <https://doi.org/10.1029/2012GL050961>.

Priestley, M. D. K., H. F. Dacre, L. Shaffrey, K. I. Hodges, and J. G. Pinto. 2018. "The Role of Serial European Windstorm Clustering for Extreme Seasonal Losses as Determined From Multi-Centennial Simulations of High-Resolution Global Climate Model Data." *Natural Hazards and Earth System Sciences* 18: 2991–3006. <https://doi.org/10.5194/nhess-18-2991-2018>.

Priestley, M. D. K., J. G. Pinto, H. F. Dacre, and L. Shaffrey. 2017. "Rossby Wave Breaking, the Upper Level Jet, and Serial Clustering of Extratropical Cyclones in Western Europe." *Geophysical Research Letters* 44: 514–521. <https://doi.org/10.1002/2016GL071277>.

Raveh-Rubin, S., Wernli, H. 2015. "Large-Scale Wind and Precipitation Extremes in the Mediterranean: A Climatological Analysis for 1979–2012." *Quarterly Journal of the Royal Meteorological Society* 141: 2404–2417. <https://doi.org/10.1002/qj.2531>.

Ridder, N. N., A. J. Pitman, S. Westra, et al. 2020. "Global Hotspots for the Occurrence of Compound Events." *Nature Communications* 11: 5956. <https://doi.org/10.1038/s41467-020-19639-3>.

Roberts, J. F., A. J. Champion, L. C. Dawkins, et al. 2014. "The XWS Open Access Catalogue of Extreme European Windstorms From 1979–2012." *Natural Hazards and Earth System Sciences* 14: 2487–2501. <https://doi.org/10.5194/nhess-14-2487-2014>.

Robson, A., and D. Reed. 1999. "Statistical Procedures for Flood Frequency Estimation." In *Flood Estimation Handbook*, vol. 3, 338. Wallingford, UK: Institute of Hydrology.

Röthlisberger, M., S. Pfahl, and O. Martius. 2016. "Regional-Scale Jet Waviness Modulates the Occurrence of Midlatitude Weather Extremes." *Geophysical Research Letters* 43: 10989–10997. <https://doi.org/10.1002/2016GL070944>.

Saville, G. 2022. *A Stormy End to Winter: Loss Estimates and Storm Science*. London, UK: WTW Insights.

Screen, J. A., R. Eade, D. M. Smith, S. Thomson, and H. Yu. 2022. "Net Equatorward Shift of the Jet Streams When the Contribution From Sea-Ice Loss Is Constrained by Observed Eddy Feedback." *Geophysical Research Letters* 49: e2022GL100523. <https://doi.org/10.1029/2022GL100523>.

Serinaldi, F., F. Lombardo, and C. G. Kilsby. 2022. "Testing Tests Before Testing Data: An Untold Tale of Compound Events and Binary Dependence." *Stochastic Environmental Research and Risk Assessment* 36: 1373–1395. <https://doi.org/10.1007/s00477-022-02190-6>.

Serinaldi, F., and S. M. Papalexiou. 2020. "Random Fields Simplified: Preserving Marginal Distributions, Correlations, and Intermittency, With Applications From Rainfall to Humidity." *Water Resources Research* 56: e2019WR026331.

Siegmund, J. F., N. Siegmund, and R. V. Donner. 2017. "CoinCalc—A New R Package for Quantifying Simultaneities of Event Seris." *Computers and Geosciences* 98: 64–72. <https://doi.org/10.1016/j.cageo.2016.10.004>.

Simpson, N. P., K. J. Mach, A. Constable, et al. 2021. "A Framework for Complex Climate Change Risk Assessment." *One Earth* 4: 489–501. <https://doi.org/10.1016/j.oneear.2021.03.005>.

Smith, K., and I. D. Phillips. 2012. "Autumn and Extended Winter Daily Precipitation Variability Over Central and Southern Scotland." *Scottish Geographical Journal* 128: 42–63. <https://doi.org/10.1080/14702541.2012.691337>.

Southern, R. L. 1979. "The Global Socio-Economic Impact of Tropical Cyclones." *Australian Meteorological Magazine* 27: 175–195.

Stalhandske, Z., C. B. Steinmann, S. Meiler, et al. 2024. "Global Multi-Hazard Risk Assessment in a Changing Climate." *Scientific Reports* 14: 5875. <https://doi.org/10.1038/s41598-024-55775-2>.

Stephan, C. C., Y. H. Ng, and N. P. Klingaman. 2018. "On Northern Hemisphere Wave Patterns Associated With Winter Rainfall Events in China." *Advances in Atmospheric Sciences* 35: 1021–1034. <https://doi.org/10.1007/s00376-018-7267-7>.

Tian, X., M. Schleiss, C. Bouwens, and N. van de Giesen. 2019. "Critical Rainfall Thresholds for Urban Pluvial Flooding Inferred From Citizen Observations." *Science of the Total Environment* 689: 258–268. <https://doi.org/10.1016/j.scitotenv.2019.06.355>.

Tucker, S. O., E. J. Kendon, N. Bellouin, E. Buonomo, B. Johnson, and J. M. Murphy. 2022. "Evaluation of a New 12 km Regional Perturbed Parameter Ensemble Over Europe." *Climate Dynamics* 58: 879–903. <https://doi.org/10.1007/s00382-021-05941-3>.

UNEP. 1992. "Agenda 21." .Technical Report, United Nations Environment Programme.

Vignotto, E., S. Engelke, and J. Zscheischler. 2021. "Clustering Bivariate Dependencies of Compound Precipitation and Wind Extremes Over Great Britain and Ireland." *Weather and Climate Extremes* 32: 100318.

Vitolo, R., D. S. Stephenson, I. Cook, and K. Mitchell-Wallace. 2009. "Serial Clustering of Intense European Storms." *Meteorologische Zeitschrift* 18: 411–424. <https://doi.org/10.1127/0941-2948/2009/0393>.

Volonté, A., S. L. Gray, P. A. Clark, O. Martínez-Alvarado, and D. Ackerley. 2024a. "Strong Surface Winds in Storm Eunice. Part 1: Storm Overview and Indications of Sting Jet Activity From Observations and Model Data." *Weather* 79: 40–45. <https://doi.org/10.1002/wea.4402>.

Volonté, A., S. L. Gray, P. A. Clark, O. Martínez-Alvarado, and D. Ackerley. 2024b. "Strong Surface Winds in Storm Eunice. Part 2: Airstream Analysis." *Weather* 79: 54–59. <https://doi.org/10.1002/wea.4401>.

Ward, P. J., J. E. Daniell, M. Duncan, et al. 2022. "Invited Perspectives: A Research Agenda Towards Disaster Risk Management Pathways in Multi-(Hazard-)risk Assessment." *Natural Hazards and Earth System Sciences* 22: 1487–1497. <https://doi.org/10.5194/nhess-22-1487-2022>.

White, A. U. 1974. "Natural Hazards, Local, National, Global." In *Natural Hazards, Local, National, Global*, edited by G. F. Gilbert, vol. 288. New York: Oxford University Press.

Wilkinson, S., S. Dunn, R. Adams, et al. 2022. "Consequence Forecasting: A Rational Framework for Predicting the Consequences of Approaching Storms." *Climate Risk Management* 35: 100412. <https://doi.org/10.1016/j.crm.2022.100412>.

Williams, G. P. 1978. "Bank-Full Discharge of Rivers." *Water Resources Research* 14: 1141–1154.

Woollings, T., M. Drouard, C. H. O'Reilly, D. M. H. Sexton, and C. McSweeney. 2023. "Trends in the Atmospheric Jet Streams Are Emerging in Observations and Could Be Linked to Tropical Warming." *Communications Earth & Environment* 4: 125. <https://doi.org/10.1038/s43247-023-00792-8>.

Woollings, T., A. Hannachi, and B. Hoskins. 2010. "Variability of the North Atlantic Eddy-Driven Jet Stream." *Quarterly Journal of the Royal Meteorological Society* 136: 856–868. <https://doi.org/10.1002/qj.625>.

Zappa, G., S. Pithan, and T. Shepherd. 2018. "Multimodel Evidence for an Atmospheric Circulation Response to Arctic Sea Ice Loss in the CMIP5 Future Projections." *Geophysical Research Letters* 54: 1011–1019. <https://doi.org/10.1002/2017GL076096>.

Zhang, X., L. Alexander, G. C. Hegerl, et al. 2011. "Indices for Monitoring Changes in Extremes Based on Daily Temperature and Precipitation Data." *WIREs Climate Change* 2: 851–870. <https://doi.org/10.1002/wcc.147>.

Zscheischler, J., P. Naveau, O. Martius, S. Engelke, and C. C. Raible. 2021. "Evaluating the Dependence Structure of Compound Precipitation and Wind Speed Extremes." *Earth System Dynamics* 12: 1–16. <https://doi.org/10.5194/esd-12-1-2021>.

Zscheischler, J., and S. I. Seneviratne. 2017. "Dependence of Drivers Affects Risks Associated With Compound Events." *Science Advances* 3: e1700263.

Zscheischler, J., S. Westra, B. J. J. M. van der Hurk, et al. 2018. "Future Climate Risk From Compound Events." *Nature Climate Change* 8: 469–477. <https://doi.org/10.1038/s41558-018-0156-3>.

Woollings, T., Hannachi, A., and Hoskins, B. 2010. "Variability of the North Atlantic Eddy-Driven Jet Stream." *Quarterly Journal of the Royal Meteorological Society*, 856–868. <https://doi.org/10.1002/qj.625>.

## Appendix: Event Sets A

### A1. Dataset Selection and Fields Used

This study uses the UK Climate Projections 2018 (UKCP18) regional simulations. On a 12km grid, over the commonly used EURO-CORDEX domain (Jacob et al. 2014), simulations were run from 1980 to 2080 using the Representative Concentration Pathway (RCP) 8.5 climate change scenario with 12 member perturbed parameter ensemble (Tucker et al. 2022). Hourly 10m instantaneous wind gusts and total precipitation were available from the 12 ensemble members for two periods (1981–2000, 2061–2080), and UKCP18r-based river flows for these two time periods have been derived (Griffin, Kay, Sayers, et al. (2024)) by using the simulated precipitation and temperature, and derived evapotranspiration, to drive the Grid-to-Grid (G2G) hydrological model (Kay et al. 2021). From these daily mean river flows output by G2G on a 1km grid over GB, a set of high-flow events was created and is openly available (Griffin, Kay, Bell, et al. 2022). A daily time-series of the area subject to extreme high flows was also provided to the authors.

Thus, UKCP18 is selected as it presents the opportunity for more extreme wind and high-flow events to be analysed than in the observational record, and for future changes to be examined. The UKCP18r simulations are argued to well represent extreme precipitation (Cotterill et al. 2021; Lane and Kay 2021; Lowe et al. 2019; Tucker et al. 2022) and wind gusts (Manning et al. 2023) when assessed against lower resolution climate model simulations and gridded historical observations. Importantly, rank correlation between GB aggregated precipitation, high-flows and extreme wind for the simulated present (1981–2000) closely matches the ~30 km resolution ERA5 reanalysis (1979–2021) (Hersbach et al. 2020) and GLOFAS river-flows derived from it using LISFLOOD (Harrigan

et al. 2023; Hirpa et al. 2018) across time windows from 1 to 180 days (Bloomfield et al. 2023). In other words, even after higher-resolution verification (i.e., against CAMELS-GB/CHESS-MET), the UKCP18r simulations appear to adequately capture co-occurrence of the extreme wind and high flows (Bloomfield et al. 2023, 2024).

### A2. Defining Widespread Hazard-Specific Events

For the present time period, 1981–1999, UKCP18r has 19 complete extended winters over 12 ensemble members, giving 228 simulated seasons designated here by the year they start in (i.e., October 1981–March 1982 is '1981'). These contain unrealised yet plausible extremes. Griffin, Kay, Bell, et al. (2022) and Griffin, Kay, Sayers, et al. (2024) used the 99.5th percentile of flow across the *whole* year ( $q_{i,j}^{99.5}$ , January–December) and required that greater than 0.1% of the area of the GB river network (19,914 grid cells, ~20 km<sup>2</sup>) exceed its threshold to constitute being within an event (blue shaded areas in Figure 2). In addition a 14-day maximum event length was imposed, and events sub-divided if flow dropped to under 1/3 of the lowest of two included peaks which were separated by at least an estimated time-to-peak of storm hydrographs. This is a point-over-threshold approach (e.g., Lechner, Simiu, and Heckert 1993; Robson and Reed 1999) and their intention was to isolate hydrologically independent, extreme and widespread events. Here, matching sets of events for extreme wind, and for completeness precipitation, are extracted.

Grids of daily totals of precipitation ( $p$ ) and maximum 10m wind gust ( $v$ ) are created, and used to define events ( $E$ ). Each event is the spatial footprint of the maxima driving that hazard (e.g.,  $v$ ) over a time-window containing an isolated hydro-meteorological extreme.

For wind events, a daily time series for  $v$  of the areal fraction of GB where it exceeds its grid cell's 98th percentile ( $v_{i,j}^{98}$ , October–March) is first computed (Figure 2). Then, the temporal limits ( $t_{\text{start}}$  and  $t_{\text{end}}$ ) of the extreme event days are defined as the first and last day of a period where this areal fraction is at least 0.1% of the whole GB land area (~300 km<sup>2</sup>). 0.1% is used for consistency with flooding (Griffin, Kay, Bell, et al. 2022), and the 98th percentile aligns with a recent consensus for wind impact estimation (e.g., Bloomfield et al. 2024; Klawa and Ulbrich 2003; Priestley et al. 2018) outlined in Appendix A3. Thus, based on these thresholds, each event consists of a sequence of consecutive extreme days, with the maximum windspeed ( $v$ ) across the duration of the event retained at each location to give an event its footprint. No wind event ever exceeds 8 days (95%  $\leq$  3 days, Figure A1), so the limit of 14 days used by Griffin, Kay, Bell, et al. (2024) and Griffin, Kay, Sayers, et al. (2022) is not needed. It is likely that clusters of two or three meteorologically distinct cyclonic systems (Mailier et al. 2006; Priestley et al. 2018; Vitolo et al. 2009) combine within longer wind events. However, the focus here is on periods of disruption as they are experienced.

Precipitation events footprints are created exactly as for wind, except that the sum of precipitation ( $p$ ) across the duration of the event is retained at each location (i.e., instead of the maximum).

### A3. Event Severity Indices

Severity indices are 'impact-based proxies' for hazards such as flooding and wind extremes (Hillier and Dixon 2020), calibrated against and designed to reflect potential damage (Bloomfield et al. 2023; e.g., Christofides et al. 1992; Heneka and Ruck 2008; Hillier and Dixon 2020; Klawa and Ulbrich 2003).

Storm Severity Indices (SSI) aim to condense the risk associated with a wind event into a single number incorporating factors thought to drive damage such as maximum wind gust ( $v$ ), area affected and duration (e.g., Christofides et al. 1992; Dorland, Tol, and Palutikof 1999; Klawa and Ulbrich 2003). Recently, following Klawa and Ulbrich (2003) a form of SSI using  $v^3$  in excess of a 98th percentile minimum threshold beneath which no damage occurs has become well-established as a norm (Bloomfield et al. 2023; e.g., Leckebusch, Renggli, and Ulbrich 2008; Osinski et al. 2016; Priestley et al. 2018). Rather than a region defined by a simple (e.g., circular) geometry (Manning et al. 2022, 2024), grid

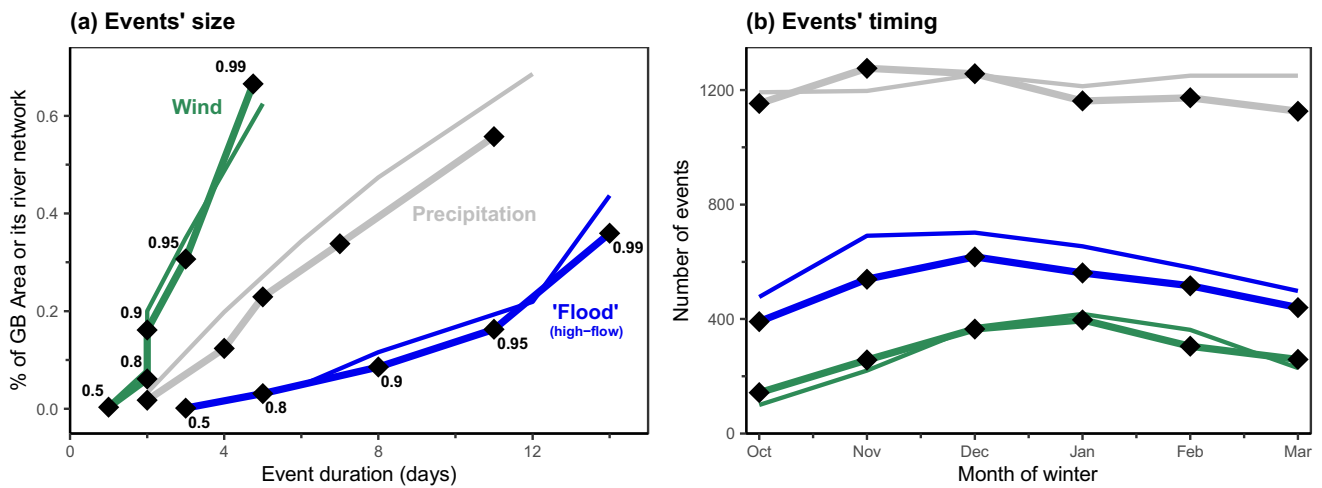


**FIGURE A1** | (a) Size and duration of events created for wind, precipitation and flood. ‘Flood’ events are high-flow events created by Griffin et al. (2023). Percentiles are shown from 50th to 99th, calculated separately for duration and area (i.e., this is not a joint distribution). Present day (thick lines) and future (thin lines) are similar if all the events are considered. (b) Seasonality of the events. [Colour figure can be viewed at [wileyonlinelibrary.com](https://wileyonlinelibrary.com)]

cells over land (e.g., Bloomfield et al. 2023; Pinto et al. 2012) are used to represent GB impact. For simplicity and to avoid a judgement linking value directly to population density (e.g., consider a wind farm), in contrast to Bloomfield et al. (2023), no population weighting is used. Thus, each event’s severity  $SSI(E)$  is given by Equation (1):

$$SSI(E) = \sum_{i=1}^{N_i} \sum_{j=1}^{N_j} \left( \frac{v(E)_{i,j}}{v_{i,j}^{98}} - 1 \right)^3 \cdot I_{i,j}$$

$$I_{i,j} = \begin{cases} 0 & \text{if } v(E)_{i,j} < v_{i,j}^{98} \\ 1 & \text{otherwise} \end{cases}$$

Two types of model have been used to approximate loss ( $l$ ) or  $SSI$ , power-law ( $l = k_1 v^\alpha$  for  $v > v_{\text{thresh}}$ ) and exponential ( $l = k_2 e^{\beta v}$ ), where  $k_1, k_2, \alpha$  and  $\beta$  are constants, parameters to be determined by fitting to loss data. In general, the challenge is to approximate data where losses rise steeply above  $\sim 32 \text{ ms}^{-1}$  (Christofides et al. 1992; Dorland, Tol, and Palutikof 1999; Heneka and Ruck 2008). Using no threshold an exponential form, which can rise very abruptly, fits postcode district losses for 5 storms better than  $\alpha$  of 2–4 (Dorland, Tol, and Palutikof 1999). With a threshold of  $\sim 20$ – $24 \text{ ms}^{-1}$  or the 98th percentile (e.g., Christofides et al. 1992; Klawa and Ulbrich 2003)  $v^3$  can fit losses for a storm (i.e., within 1–2 days) at district or national resolution, and allow modelling of district level historical losses (e.g., Pinto et al. 2012). This said, the 1999 storms sequence (Anatol, Lothar and Martin) showed losses above  $24 \text{ ms}^{-1}$  may on occasion rise more sharply for certain domains (i.e.,  $v^4 - v^5$  for Denmark, Germany) (MunichRe 2002).

At a daily timescale a 98 percentile threshold (i.e.,  $\sim 7$  times per year) arises as, in practice, relatively little damage occurs below this level ( $\sim 20 \text{ ms}^{-1}$ ) in the flat areas of UK and German (Klawa and Ulbrich 2003; Palutikof and Skellern 1991). Of course some places, such as mountains, are windier (Heneka et al. 2006; e.g., Hewston and Dorling 2011) but both nature (e.g., trees) and the built environment appear to adapt to this recurrence level. Klawa and Ulbrich (2003) illustratively note that winds at List (island of Sylt) exceed  $20 \text{ ms}^{-1}$  1-in-5 days to no noticeable detriment, and building regulations (e.g., UK, Germany, Netherlands) require greater resilience in windier areas (e.g., Böllman and Jurksch 1984; Chandler, Jones, and Patel 2001; Dorland, Tol, and Palutikof 1999; Hill, Gatley, and Peiris 2013). Whilst a higher percentile might be appropriate for higher frequency data (6-hourly, 99th) (Manning et al. 2024), damage on 2% of days (i.e., 98th percentile) is not wildly different from the

number of UK storms, which are named (i.e., 7–8 per/year) when the Met Office believes it has ‘potential to cause disruption or damage’ (Met Office 2024).

Probabilistic models account for the uncertainty in how individual assets are damaged (Heneka et al. 2006; Heneka and Ruck 2008), for instance using a power-law and replacing the threshold with a function describing the probability of damage (Pardowitz et al. 2016; Prahl et al. 2012). This better approximates losses in Germany across all 2004 wintertime days in 11 years (1997–2007), although the costliest days ( $\sim 10$  per year) are still adequately modelled using cubic excess-over-threshold approach with a 98th percentile (Prahl et al. 2015). Thus using Equation (1) is appropriate as these ‘extremes’ are the focus of this paper, particularly as ranks rather than absolute  $SSI$  values are primarily evaluated. Moreover, sensitivity testing indicates limited sensitivity of patterns of correlation (e.g., spatial) to the choice of threshold (Hillier and Dixon 2020), something borne out by the convergence of results for recent UK flood-wind research that have employed a spectrum of methodological choices (see Section 4.1).

Storm duration has been argued to influence losses (e.g., Christofides et al. 1992), but statistical studies have found that it does not improve models and may risk ‘over-fitting’ (Dorland, Tol, and Palutikof 1999), so in line with the Klawa and Ulbrich (2003) such potential influences (e.g., precipitation, duration) are not included here. We also note that  $v^3$  is theoretically related to kinetic energy flux (e.g., Pinto et al. 2012) and to the dissipation of kinetic energy in the surface layers of a storm (Bister and Emanuel 1998; Businger and Businger 2001; Emanuel 1998, 2005). However, we discount this as any justification for a cubic relationship between economic loss and  $v$ , other than perhaps as for the presence of non-linearity. Simply, for cubically increasing losses over a threshold (e.g., Christofides et al. 1992; Dorland, Tol, and Palutikof 1999) a cubic relationship that starts at zero velocity, as kinetic energy must, does not fit them well (Prahl et al. 2015).

Based on the form of  $SSI$ , Flood Severity Indices (FSI) have recently been developed (Bloomfield et al. 2023, 2024). Only grid cells on the river network (e.g., Bloomfield et al. 2023) are used, again with no population weighting. Thus, each events’ flood severity  $FSI(E)$  is given by Equation (2):

$$FSI(E) = \sum_{i=1}^{N_i} \sum_{j=1}^{N_j} \left( \frac{q(E)_{i,j}}{q_{i,j}^{99.5}} - 1 \right) \cdot I_{i,j}$$

$$I_{i,j} = \begin{cases} 0 & \text{if } q(E)_{i,j} < q_{i,j}^{99.5} \\ 1 & \text{otherwise} \end{cases}$$

**TABLE A1** | Table of thresholds or limits used to define events. These thresholds used (i) in defining events and (ii) calculating severity indices are not to be confused with the percentiles used to distinguish events of differing severity in the Results (e.g., 75th percentile of events once they have been isolated and quantified in terms of a severity index).

| Threshold/limit  | Value   |
|--|---------|
| Percent of river network ( $q$ )   | 0.1%    |
| Percent of GB land area ( $v, p$ )   | 0.1%    |
| Extreme peak river flow (whole year), percentile of daily values             | 99.5%   |
| Extreme precipitation (October–March), percentile of daily values            | 98.0%   |
| Extreme daily 10 m max wind gust (October–March), percentile of daily values | 98.0%   |
| Maximum length of event—from Griffin, Kay, Bell, et al. (2022)               | 14 days |

The 99.5th percentile is inherited, for consistency, from Griffin, Kay, Bell, et al. (2022). It is largely arbitrary, intended to yield sufficient data points for statistical analysis (Bloomfield et al. 2023; Griffin, Kay, Sayers, et al. (2022); Martius, Pfahl, and Chevalier 2016; Zhang et al. 2011). It is less than the 2-year return period ‘rule of thumb’ for bank-full discharge (i.e., 99.9th percentile), although the work this derives from Williams (1978) is highly equivocal (i.e., 1–32 year range) due to factors such as basin characteristics, local climate and flood defences (Berghuijs et al. 2019; e.g., Tian et al. 2019). The cubic power is removed as it is not required with, as for SSI, justification of this functional form of FSI being through validation, replicating losses and capturing known floods (Bloomfield et al. 2023). Historical FSIs are highly correlated ( $r=0.74$ ,  $p<0.05$ ) with infrastructure loss data on an annual timescale, and FSI captures 28 of 34 wintertime floods (1980–2020) in the Chronology of British Hydrological Events (Black and Law 2004). This said, lots of small FSI ‘events’ occur where no flooding was historically recorded. Also, without a threshold non-linearity (i.e.,  $SI^{-5}$ ) improves the fit of one proxy to losses (Hillier and Dixon 2020), so debate on the form of FSI is expected to continue.

FSI as configured in Equation (2) is suitable here as only the most extreme events are selected (i.e.,  $>75$ th percentile of events). This is 5–6 high flows per year, comparable to the ~7 floods per year in commercial risk models (Hillier et al. 2024).

A Precipitation Severity Index (PSI) is used for consistency, despite severity perhaps being an incorrect term as rain itself rarely does damage directly (Manning et al. 2024). PSI is defined as for SSI, except that a cubic relationship is omitted as there is no justification for the additional complexity. PSI( $E$ ) for each event is given by Equation (3):

$$PSI(E) = \sum_{i=1}^{N_i} \sum_{j=1}^{N_j} \left( \frac{p(E)_{ij}}{p_{ij}^{98}} - 1 \right) \cdot I_{ij}$$

$$I_{ij} = \begin{cases} 0 & \text{if } p(E)_{ij} < p_{ij}^{98} \\ 1 & \text{otherwise} \end{cases}$$

#### A4. Description of Event Sets

A set of high-flows events (Griffin, Kay, Bell, et al. 2022; Griffin, Kay, Sayers, et al. 2024) has been created for the UKCP18 12-member perturbed parameter ensemble (PPE) of the Hadley Centre 12 km Regional Climate Model (RCM) (Murphy et al. 2018; Tucker et al. 2022). Thus, to mirror this, UKCP18r was used to generate wind ( $n=3427$ ) and precipitation ( $n=14,502$ ) events across mainland Great Britain for baseline (winters 1981–1999) and future (winters 2061–2079) time-slices. The

wind event set is broadly aligned to other such sets in its construction methods (Lockwood et al. 2022; Osinski et al. 2016; Roberts et al. 2014), and the data been validated for the purposes of examining hazard co-occurrence (Appendix A1). Summary metrics are created for these event footprints (total area, duration and SI) and assigned to a single date  $t_{\max}$ , the individual day when the greatest number of grid cells exceed the set threshold.

First consider the size and number of events at the present time. There are 7–8 wind events per year in 1981–1999 on average, each tending to affect a large area (i.e., up to 60% of GB) but be relatively short-lived (<5-day). This contrasts longer-duration yet more localised fluvial flooding (Figure A1a). These properties match what is typical of these event types (e.g., Mitchell-Wallace et al. 2017). No wind event ever exceeds 8 days, so the limit of 14 days used by Griffin, Kay, Bell, et al. (2022) and Griffin, Kay, Sayers, et al. (2024) is not needed. Extreme precipitation is more common than wind with 31–33 events per year, as is flooding at 13–16 events per year.

The relative frequency of events is statistically dictated, depending upon the size of each phenomenon and the parameters (e.g., thresholds) used to extract events. The spatial length-scale of correlation (i.e., floods are typically smaller) increases their number, counteracted somewhat by them lasting longer and the higher percentile. Imagine an idealised scenario wherein windstorms hit the whole United Kingdom, while floods impact 10% of its area (e.g., in 10 uncorrelated areas). Now, for a 98th daily percentile, every 1 in 50 days all WS points will peak at the same time giving 1 event. For flood, this will happen separately in the 10 areas, giving 10 events. The higher percentile (i.e., 99.5th vs. 98th) used for flooding will reduce this by four times, giving 2.5 events in 50 days. Also, by lasting longer, the flood events might merge more readily, reducing their number.

The events in 2061–2079 have some differences to 1981–1999. Figure A1 echoes the finding of Griffin, Kay, Sayers, et al. (2022) that flooding is expected to be more frequent (+18% here) and heavier tailed with larger extreme events (Figure A1a) and somewhat more seasonal with a focus in mid-winter (DJF), but also identifies a potential shift to a slightly earlier peak in future (Figure A1b). Considering all events, neither precipitation nor wind events increase in number significantly into the future ( $t$  test between means of ensemble members), and echoes the muted changes in climatology (e.g., Manning et al. 2022, 2024). It differs, however, from true extremes are examined in papers (Bloomfield et al. 2023) or the main text. Illustratively, increases for Oct–Mar are +59% for the 75th percentile of FSI, +91% for the 95th percentile of FSI in Figure 6a,d, both of which are significant ( $p<0.01$ ).

Only the top quarter of events defined are focussed upon (i.e., most severe quarter,  $>75$ th percentile). For wind events there are 7–8 per year in total, which roughly reflects the Met Office’s named storms 2015–2023 (7.4 per year) (Met Office 2024). Thus, 1–2 per year are focussed upon, comparable to the ~3 per year used in insurance industry risk modelling (Hillier et al. 2024). There are 15 high flow events per year, and taking the top quarter gives ~4 notable high-flow events, comparable to the 6–7 floods per year in a commercial model (Hillier et al. 2024).

#### Appendix: Additional Statistics B

##### B1. For Increased Concentration of Events and Episodes in Midwinter

In Section 3.2, from Figure 6, claims are made about an increased concentration of flooding, extreme wind and episodes containing both in midwinter. Table A1 presents a statistical analysis of the prevalence of events and episodes between December and February (DJF) as compared to the whole October–March winter. A Binomial distribution is used, that is,  $X \sim B(t, f)$ , with  $t$  trials and a chance of success  $f$ . Then using the cumulative Binomial distribution, the chance of the observed number of events (i.e.,  $n$  in DJF) or more arising through random selection within in a stated number of trials (i.e.,  $n$  in whole winter) can be assessed. First, the hypothesis that there are more events in DJF is tested. Here the null hypothesis is that the real distribution in time is equal between DJF and the three other months, that is,  $f=0.5$ . With

**TABLE B1** | Table presenting a statistical analysis of the prevalence of events and episodes between December and February (DJF) as compared to the whole October–March winter.

|                     |        |                      |         | Total, <i>n</i> | DJF, <i>n</i> | Fraction ( <i>f</i> ) DJF | <i>p</i> ( <i>f</i> =0.5) | <i>p</i> ( <i>f</i> =present day) |
|---------------------|--------|----------------------|---------|-----------------|---------------|---------------------------|---------------------------|-----------------------------------|
| Single events       | 3-day  | Flood                | Present | 766             | 488           | 0.637                     | 0.000                     | —                                 |
|                     |        |                      | Future  | 1197            | 747           | 0.624                     | 0.000                     | 0.818                             |
|                     |        | Wind                 | Present | 432             | 267           | 0.618                     | 0.000                     | —                                 |
|                     | 21-day | Flood                | Present | 450             | 328           | 0.729                     | 0.000                     | 0.000                             |
|                     |        |                      | Future  | 154             | 102           | 0.662                     | 0.000                     | —                                 |
|                     |        | Wind                 | Present | 266             | 199           | 0.748                     | 0.000                     | 0.001                             |
|                     |        | Future               | 87      | 52              | 0.598         | 0.027                     | —                         |                                   |
| Flood-wind episodes | 3-day  | $\varepsilon_W^{75}$ | Present | 155             | 103           | 0.665                     | 0.000                     | —                                 |
|                     |        | $\varepsilon_W^{75}$ | Future  | 309             | 228           | 0.738                     | 0.000                     | 0.002                             |
|                     | 21-day | $\varepsilon_W^{95}$ | Present | 51              | 34            | 0.667                     | 0.005                     | —                                 |
|                     |        | $\varepsilon_W^{95}$ | Future  | 83              | 71            | 0.855                     | 0.000                     | 0.000                             |

*p* < 0.05 in all cases (Table B1), the research hypothesis that events and episodes are concentrated in midwinter can be accepted. Second, the hypothesis that levels of concentration in midwinter are increasing from 1981–1999 to 2061–2079 is tested. Here, *f* is set by the fraction of events in DJF in the present day. In all cases except lower-percentile (75th) for 3-day flooding, events and episodes are significantly (*p* < 0.05) more concentrated in midwinter (i.e., DJF).